CDK4 Phosphorylates AMPK2 to Inhibit Its Activity and Repress Fatty Acid Oxidation

Lopez-Mejia, Isabel C.; Lagarrigue, Sylviane; Giralt, Albert; Martinez-Carreres, Laia; Zanou, Nadège; Denechaud, Pierre-Damien; Castillo-Armengol, Judit; Chavey, Carine; Orpinell, Meritxell; Delacuisine, Brigitte; Nasrallah, Anita; Collodet, Caterina; Zhang, Lianjun; Viollet, Benoît ; Hardie, D. Grahame; Fajas, Lluis

Published in:
Molecular Cell

DOI:
10.1016/j.molcel.2017.09.034

Publication date:
2017

Document Version
Peer reviewed version

Accepted Manuscript

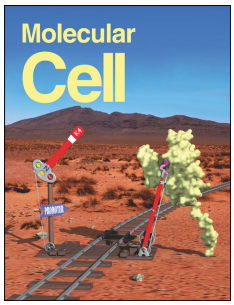

CDK4 phosphorylates AMPK*α*2 to inhibit its activity and repress fatty acid oxidation

Isabel C. Lopez-Mejia, Sylviane Lagarrigue, Albert Giralt, Laia Martinez-Carreres, Nadège Zanou, Pierre-Damien Denechaud, Judit Castillo-Armengol, Carine Chavey, Meritxell Orpinell, Brigitte Delacuisine, Anita Nasrallah, Caterina Collodet, Lianjun Zhang, Benoît Viollet, D. Grahame Hardie, Lluis Fajas

PII: S1097-2765(17)30712-8

DOI: 10.1016/j.molcel.2017.09.034

Reference: MOLCEL 6393

To appear in: *Molecular Cell*

Received Date: 14 November 2016

Revised Date: 17 July 2017

Accepted Date: 22 September 2017

Please cite this article as: Lopez-Mejia, I.C., Lagarrigue, S., Giralt, A., Martinez-Carreres, L., Zanou, N., Denechaud, P.-D., Castillo-Armengol, J., Chavey, C., Orpinell, M., Delacuisine, B., Nasrallah, A., Collodet, C., Zhang, L., Viollet, B., Hardie, D.G., Fajas, L., CDK4 phosphorylates AMPK*α*2 to inhibit its activity and repress fatty acid oxidation, *Molecular Cell* (2017), doi: 10.1016/j.molcel.2017.09.034.

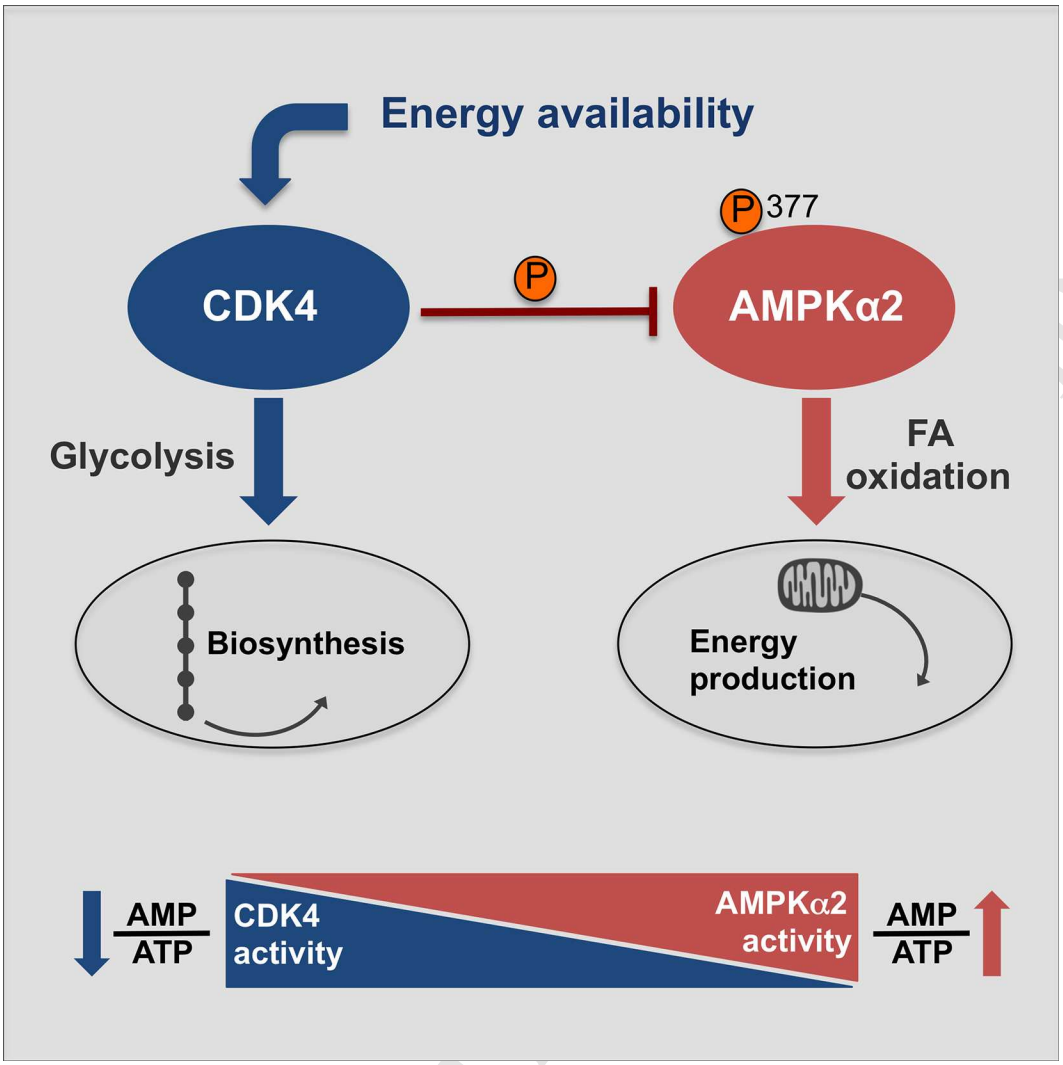

Highlights

- CDK4 promotes glycolysis and inhibits fatty acid oxidation
- CDK4 inhibits AMPK activity through direct phosphorylation of the AMPK- α2 subunit.
- CDK4-/- mice have AMPK-dependent increased oxidative metabolism

eTOC Blurb

Lopez-Mejia et al. show in this study that CDK4, a protein that is usually involved in the control of cell division, is an important regulator of the energy balance of the cell through the direct inhibition of the activity of AMPK, which is a major regulator of energy consuming processes.

CDK4 phosphorylates AMPKα2 to inhibit its activity and repress fatty acid oxidation

Isabel C. Lopez-Mejia[1,2], Sylviane Lagarrigue[2], Albert Giralt[1], Laia Martinez-Carreres[1], Nadège Zanou[2,3], Pierre-Damien Denechaud[1,2], Judit Castillo-Armengol[1], Carine Chavey[4], Meritxell Orpinell[2], Brigitte Delacuisine[1,2], Anita Nasrallah[1], Caterina Collodet[5,6], Lianjun Zhang[7], Benoît Viollet[8,9,10], D. Grahame Hardie[11] and Lluis Fajas[1,2*]

[1]Center for Integrative Genomics, University of Lausanne, 1015 Lausanne, Switzerland

[2]Department of Physiology, University of Lausanne, 1005 Lausanne, Switzerland

[3]Institute of Sport Sciences, University of Lausanne, 1015 Lausanne, Switzerland

[4]IGMM, Université de Montpellier, UMR 5535 CNRS, F-34293, France

[5]Nestlé Institute of Health Sciences SA, EPFL Innovation Park, 1015 Lausanne, Switzerland.

[6]École Polytechnique Fédérale de Lausanne, School of Life Sciences, 1015 Lausanne, Switzerland.

[7]Ludwig Center for Cancer Research, University of Lausanne, 1066 Epalinges, Switzerland

[8] Institut Cochin, INSERM U1016, Paris, France.

[9]CNRS, UMR 8104, Paris, France.

[10] Université Paris Descartes, Sorbonne Paris Cité, Paris, France.

[11]School of Life Sciences, University of Dundee, Dundee, Scotland, UK

[*] Corresponding author

Lead Contact: Pr. Lluis Fajas

Email: Lluis.Fajas@unil.ch

Abstract

The roles of CDK4 in the cell cycle have been extensively studied, however less is known about the mechanisms underlying the metabolic regulation by CDK4. Here, we report that CDK4 promotes anaerobic glycolysis and represses fatty acid oxidation in mouse embryonic fibroblasts (MEFs) by targeting the AMP-activated protein kinase (AMPK). We also show that fatty acid oxidation (FAO) is specifically induced by AMPK complexes containing the α2 subunit. Moreover, we report that CDK4 represses FAO through direct phosphorylation and inhibition of AMPKα2. The expression of non-phosphorylatable AMPKα2 mutants, or the use of a CDK4 inhibitor, both increased FAO rates in MEFs and myotubes. In addition, *Cdk4*$^{-/-}$ mice have increased oxidative metabolism and exercise capacity. Inhibition of CDK4 mimicked these alterations in normal mice, but not when skeletal muscle was AMPK-deficient. This novel mechanism explains how CDK4 promotes anabolism by blocking catabolic processes (FAO) that are activated by AMPK.

Introduction

Promitotic signals such as growth factors increase the levels of D-type cyclins (cyclin D1, D2 and D3), which bind and activate CDK4/6 to trigger the phosphorylation of the retinoblastoma-associated protein pRB and other pocket proteins, i.e. p107 and p130 (Malumbres and Barbacid, 2005). Rb phosphorylation enables release of the E2F transcription factors that promote the transcription of genes necessary for the replication of the genome (Malumbres and Barbacid, 2005). The role of CDK4 in the regulation of cell cycle progression has been extensively studied in eumetazoan organisms, and alterations in CDK4 activity have been associated with cancer development and progression (Malumbres and Barbacid, 2001, 2009; O'Leary et al., 2016). For example, the R24C mutation, which is used in this study, renders CDK4 resistant to inhibition by INK4 inhibitors and has been reported to confer a genetic predisposition to melanoma (Rane et al., 2002; Rane et al., 1999; Wolfel et al., 1995).

Cell division requires substantial amounts of ATP, and numerous metabolic intermediates to support biosynthesis of essential molecules, such as lipids and nucleic acids. Proliferating cells preferentially use anaerobic glycolysis to generate large amounts of ATP, and to provide metabolic intermediates to support cell growth (Jones and Thompson, 2009). Growing evidence demonstrates that regulatory crosstalk exists between metabolic pathways and regulators of cell cycle progression. Mitochondrial respiration and metabolism are coordinated with cell cycle progression by cell cycle regulators (Lopez-Mejia and Fajas, 2015; Salazar-Roa and Malumbres, 2016)). Our laboratory and others have demonstrated that CDK4 is one such “metabolic” cell cycle regulator (Blanchet et al., 2011; Icreverzi et al., 2012; Lagarrigue et al., 2016; Lee et al., 2014). Indeed, we have previously shown that CDK4 regulates oxidative metabolism via the E2F1 transcription factor, in muscle and brown adipose tissue (Blanchet et al., 2011) and promotes the insulin-signaling pathway in mature adipocytes (Lagarrigue et al., 2016). Overall, the participation of cell cycle regulators in the control of energy homeostasis occurs mainly through the activation of anabolic processes (Aguilar and Fajas, 2010). The AMP-activated protein kinase (AMPK) is a central inhibitor of such anabolic processes and might therefore be repressed by cell-cycle regulators.

Under conditions of low cellular energy, AMP and ADP are increased relative to ATP, and this is sensed by AMPK. AMPK exists as heterotrimeric complexes composed of a catalytic subunit, α, and two regulatory subunits, β and γ; the α and β subunits exist as two isoforms (α1/α2 and β1/β2, encoded by the *PRKAA1/2* and *PRKAB1/2* genes), and the γ subunit as three isoforms (γ1/γ2/γ3, encoded by *PRKAG1/2/3*), thus generating up to 12 combinations of heterotrimeric complex (Carling, 2004; Grahame Hardie, 2016; Hardie et al., 2012; Ross et al., 2016b). AMPK is regulated both by phosphorylation/dephosphorylation and by the relative cellular concentrations of adenine nucleotides, with the two mechanisms being intimately linked. Firstly, the upstream kinases LKB1 (liver kinase B1) (Hawley et al., 2003; Shaw et al., 2004; Woods et al., 2003) or CaMKK2 (calmodulin-dependent kinase kinase-2/-β) (Hawley et al., 2005; Hurley et al., 2005; Woods et al., 2005) activate AMPK through the phosphorylation of Thr^{172} of the α subunit (Hawley et al., 1996). Secondly, AMPK is regulated through the competitive binding of ATP, or AMP and ADP at up to three sites on the γ subunit. When cellular energy levels are low, binding of AMP or ADP enhances Thr^{172} phosphorylation by LKB1 and inhibits Thr^{172} dephosphorylation by protein phosphatases, while binding of AMP (but not ADP) causes further allosteric activation (Ross et al., 2016a). Metabolic stresses that reduce intracellular ATP concentrations are therefore the best-characterized activators of AMPK, although it has recently been shown that glucose deprivation can activate AMPK by an adenine nucleotide-independent mechanism (Zhang et al., 2017). Once activated, AMPK promotes catabolic pathways that generate ATP (e.g. fatty acid oxidation, FAO) while switching off anabolic pathways and other ATP-requiring processes to restore cellular ATP levels (Carling, 2004; Grahame Hardie, 2016; Hardie et al., 2012; Ross et al., 2016b).

Other kinase activities that are induced by growth stimuli are known to inhibit AMPK. This includes AKT a key effector of the insulin/IGF1-signaling pathway that antagonizes the AMPK pathway through phosphorylation of AMPKα1 on Ser^{487} (Horman et al., 2006b), or ERK, that was shown to phosphorylate the same residue (Lopez-Cotarelo et al., 2015). The cyclic AMP-dependent protein kinase (PKA) also phosphorylates and negatively regulates AMPK (Djouder et al., 2010; Hurley et al., 2006), and Thr^{481} and Ser^{477} on AMPKα1 are phosphorylated

by glycogen synthase kinase 3 (GSK3)(Suzuki et al., 2013), following a "priming" phosphorylation of Ser^{487} by AKT.

Muscle function requires a finely tuned balance between anabolism and catabolism in order to respond to physiological challenges within the available energy supply. AMPK is a major coordinator of energy intake and utilization in exercising muscle (Hoffman et al., 2015), functioning to enhance energy availability. Amongst other effects, AMPK promotes FAO to maintain ATP cellular stores, although the exact role of AMPK in regulation of muscle FAO has been controversial (Mounier et al., 2015).

In this study, we sought to determine whether CDK4 participates in energy homeostasis by inhibiting catabolic processes. The mechanisms by which the activity of AMPK is inhibited under anabolic conditions, such as during cell cycle progression or in resting muscle, have not been thoroughly studied. We report here that CDK4 enhances anaerobic glycolysis and represses fatty acid oxidation. Surprisingly, the AMPKα1 and α2 subunits play distinct roles. We provide here a molecular mechanism whereby CDK4-CycD3 complexes directly repress α2-containing complexes to inhibit FAO. We show that chemical and genetic inhibition of CDK4 also promotes oxidative metabolism *in vivo*, as evidenced by decreased respiratory exchange ratio (RER) and increased exercise performance in mice lacking CDK4 activity.

Results

CDK4 modulates FAO in an E2F1-independent manner

We previously demonstrated that CDK4 is a major mediator of insulin signaling, and therefore contributes to the positive regulation of biosynthetic processes, such as fatty acid synthesis, and the inhibition of catabolic pathways, such as lipolysis (Lagarrigue et al., 2016). To further investigate the contribution of CDK4 to metabolic regulation, Seahorse analyses were performed. *Cdk4*$^{R24C/R24C}$ mouse embryonic fibroblasts (MEFs), which express a hyperactive CDK4 mutant, exhibited a significant increase in anaerobic glycolysis, as measured by the extracellular acidification rate (ECAR), whereas *Cdk4*$^{-/-}$ MEFs had impaired anaerobic glycolysis (Figures 1a-b). In contrast, CDK4 activity was inversely correlated with FAO. *Cdk4*$^{R24C/R24C}$ MEFs metabolized palmitate at a low rate, whereas *Cdk4*$^{-/-}$ MEFs showed increased palmitate oxidation (Figures 1c-d). Interestingly, the effects of CDK4 on substrate use were independent of E2F1 activity, since deletion of E2F1 in *Cdk4*$^{R24C/R24C}$ MEFs failed to reverse the effects of *Cdk4*^{R24C} on anaerobic glycolysis or palmitate oxidation (Figures 1e-h). These results suggest that CDK4 controls substrate utilization in MEFs independently of E2F1.

CDK4 regulation of FAO is AMPK-dependent

The decrease in FAO observed in response to constitutive activation of CDK4 is opposite to the effect seen with AMPK activation (Fullerton et al., 2013; Hardie, 2015; Hardie and Pan, 2002; O'Neill et al., 2014). Therefore, we analyzed the involvement of AMPK in the CDK4-mediated regulation of FAO in MEFs. Basal levels of phosphorylated ACC (pACC), which is a known target and marker of AMPK activity, were decreased in *Cdk4*$^{R24C/R24C}$ MEFs but increased 3-fold in the *Cdk4*$^{-/-}$ cells (Figures 2a-b and S1a-b), suggesting that CDK4 antagonizes AMPK function. Moreover, the activation of AMPK by the specific activator A769662 (Goransson et al., 2007; Moreno et al., 2008) was reduced in *Cdk4*$^{R24C/R24C}$ MEFs (Figures 2a-b), suggesting that CDK4 can prevent AMPK activation. In addition, increased AMP/ATP and ADP/ATP ratios were observed in MEFs expressing the hyperactive CDK4 mutant, which suggested a lower catabolic rate (Figures 2c-d). Interestingly, in *Cdk4*$^{-/-}$ MEFs, comparable pACC levels were measured both in the

basal state and upon AMPK stimulation (Figures 2a-b). This finding implies that in the absence of CDK4, AMPK reaches its activated state without need for any further stimulation. Likewise in *Cdk4*$^{-/-}$ cells, and in WT MEFs treated with A769662, we observed a significant decrease of AMP/ATP and ADP/ATP ratios (Figures 2 c-f).

Next, we studied the physiological relevance of the increase in AMPK activity in *Cdk4*$^{-/-}$ cells, using FAO assays in MEFs treated with A769662 and with the non-selective AMPK inhibitor Compound C. As expected, the levels of palmitate oxidation in WT MEFs were at least 25% higher in A769662-treated cells (Figures 2g and S1c-d). However, *Cdk4*$^{-/-}$ cells did not respond in the same assay to A769662 treatment. By contrast, AMPK activation by A769662 in *Cdk4*$^{R24C/R24C}$ MEFs was only able to restore WT levels of FAO (Figures 2g and S1c-d). AMPK inhibition in *Cdk4*$^{-/-}$ cells (albeit by the non-selective inhibitor compound C) produced consistent results. The levels of pACC in CDK4 null MEFs, as well as the increased FAO levels were restored back to basal levels (Figures S1e-g). Taken together, these results suggest that CDK4 inhibits the AMPK pathway.

The AMPKα2 subunit is required for efficient FAO in MEFs

Our results suggested that CDK4 has a negative effect on FAO via the regulation of AMPK activity, raising the question of which AMPK subunits contribute to this effect. Interestingly, the deletion of either AMPKα subunit in MEFs resulted in increased ECAR, indicating increased glycolysis, whereas the complete abrogation of AMPK activity had no effect, perhaps due to disruption of glucose transport into the cells (Figures 3a-b). However, although AMPKα1KO MEFs metabolized palmitate as efficiently as control cells, both AMPKα2KO and AMPK α1/ α2KO (DKO) cells exhibited significantly reduced levels of FAO (Figures 3c-d). Consistently, A769662 failed to trigger FAO in cells lacking the α2 subunit (both α2KO and DKO). Thus, despite being more abundant in MEFs (Morizane et al., 2011), the AMPKα1 subunit cannot substitute for the α2 subunit in the control of FAO, even when allosterically activated by A769662 (Figures 3e-f and S1h-i). In addition, ACC phosphorylation could be detected upon stimulation with A769662 in both AMPK α1KO and AMPK α2KO MEFs (Figure S1j), suggesting that both AMPK subunits can phosphorylate ACC1 and therefore inhibit lipid synthesis, but

only AMPKα2 can promote FAO. Taken together, these results suggest that AMPK complexes containing α2 specifically control FAO.

CDK4 phosphorylates the AMPK α2 subunit

The inhibition of AMPKα2-dependent FAO could be the result of a direct phosphorylation by CDK4. *In vitro* kinase assays showed that recombinant CDK4/CycD3 phosphorylated all GST fusions of AMPK subunits tested at different levels (Figure 4a, loading control in S2a). Interestingly, AMPKα2 and AMPK γ 2 were phosphorylated by CDK4 to a greater extent than pRB, which is the canonical CDK4 substrate (Figure 4b). Since the specificity of CDKs is partially determined by substrate docking on the cyclin subunit, kinase assays were also performed using recombinant CDK4/CycD1 instead of CDK4/CycD3. The phosphorylation of the AMPK subunits was very low under these conditions (Figure S2b), suggesting that AMPK phosphorylation by CDK4 requires recognition by cyclin D3.

AMPKα2 was predicted to contain 6 CDK4 phosphorylation sites (Thr^{85}, Ser^{176}, Ser^{345}, Ser^{377}, Thr^{485}, Ser^{529}). Out of these six potential sites, five were listed in the phosphoNET database (Figure 4c). Site-directed mutagenesis (S>A or T>A) combined with protein truncation studies (Figure S3c) identified Ser^{345}, Ser^{377}, Thr^{485} and Ser^{529} as CDK4 phosphorylation sites (Figures 4d-e, loading control in S3d). Phosphorylation by CDK4 was completely abrogated in a full-length recombinant protein carrying Ser to Ala or Thr to Ala mutations at the four CDK4 phosphosites (α2 S>A mutant), suggesting that the four newly-identified residues account for all sites phosphorylated on GST-AMPKα2 by CDK4 in cell-free assays (Figure 4f-g, loading control in S2e). The phosphorylation of Ser^{377} and Thr^{485} have been previously described in proteomic studies (Figure S2f) (Dinkel et al., 2011; Gnad et al., 2011; Hornbeck et al., 2015)), including cell cycle-related phosphoproteomes (Daub et al., 2008; Kettenbach et al., 2011), and in liver upon insulin stimulation (Humphrey et al., 2015), suggesting that the regulation of AMPK by CDK4 is important for cell cycle progression and for the insulin signaling pathway. Moreover, we found the four newly identified CDK4 phosphosites to be conserved among the AMPKα2 subunits of several mammalian species (Figure S3a) but not between the AMPKα*1* and AMPKα2 isoforms (Figure S3b).

In intact cells, AMPK is found as a heterotrimeric complex; therefore recombinant kinase-inactive α2β2γ1 complexes were also used as substrate for recombinant CDK4/CycD3 complexes. After mass spectrometry analysis we obtained 83 % coverage of the AMPKα2 subunit and observed the phosphorylation in Ser^{176} and Ser^{377} (Figure 4h). A targeted analysis to increase coverage showed phosphorylation of Thr^{485} and Ser^{529} with low detectability. The phosphorylation of Ser^{345} and Ser^{377} was also detected in myotubes and muscle tissue, which express high levels of the α2 subunit (Figures S4a-b and table S1). Interestingly, our results suggest that these phosphorylations are present when AMPK is inactive since the activating Thr^{172} phosphorylation was not found in 5 out of 6 experiments (Figures S4a-b). Taken together, these data indicate that the α2 subunit of AMPK is a substrate for CDK4-CycD3 complexes in cell-free assays, and that some of these phosphorylations occur *in vivo*, in conditions in which CDK4 is active (Blanchet et al., 2011; Lagarrigue et al., 2016), but AMPK is inactive.

AMPKα2 phosphorylation is necessary and sufficient for FAO repression by CDK4

To elucidate the functional relevance of the phosphorylation of AMPKα2 by CDK4, we compared the regulatory activities of AMPKα2 S>A, AMPKα2 and AMPKα1 in the context of FAO. Transfection of AMPK DKO MEFs with the AMPKα2 S>A mutant conferred ACC phosphorylation levels that where higher than those observed in AMPKα1- or α2-transfected cells both in the basal state and upon stimulation by A769662 (Figure 5a). Similarly, ectopic expression of the AMPKα2 S>A mutant in the FAO-defective AMPK DKO MEFs rescued palmitate oxidation to a greater extent than that which was observed upon transfection with WT AMPKα2 (Figures 5b and S5a). Taken together, these results indicate that defective targeting of AMPKα2 by CDK4 at Ser^{345}, Ser^{377}, Thr^{485} and Ser^{529} results in increased AMPKα2 FAO-promoting activity.

In order to demonstrate that CDK4 represses FAO by repressing AMPK activity, wild type and AMPK mutant cells were treated with CDK4 inhibitors. Inhibition of CDK4 activity by LY2835219 significantly increased FAO, after 24 hours (Figures 5c and S5b) or 2 hours (Figures S5c-d) of treatment. Strikingly, the CDK4 inhibitor failed to increase FAO in both AMPK α2KO or AMPK DKO cells but

not in AMPK α1KO cells, demonstrating that CDK4 targets AMPKα2 to alter cellular metabolism (Figures 5c, S5b and S5e-g). The overall positive effect of CDK4 inhibition on AMPK activity was confirmed by analyzing ACC phosphorylation. Indeed, LY2835219 treatment induced a dose-dependent increase in the phosphorylation of ACC (Figures S5h and S5i). This effect correlated with decreased CDK4 activity given that phosphorylation of RB Ser^{780} was also reduced (Figures S5i). Of note, increased ACC phosphorylation and increased FAO could be detected after 2h of CDK4 inhibition, whereas inhibition of RB phosphorylation required longer treatments. Moreover, LY2835219 had a comparable effect as A769662, significantly decreasing AMP/ATP and ADP/ATP ratios in WT MEFs (Figures 2e-f and 5d-e). The use of LY2835219 suggests that CDK4 inhibition promotes catabolic processes in an AMPKα2-subunit dependent manner.

We next decided to validate our finding in a more physiological cellular model. LY2835219 treatment induced an increase in FAO in C2C12 myotubes, which are known to express high levels of AMPKα2 (Figures S6a-b). In this model, CDK4 inhibition correlated with a dose-dependent increase of the phosphorylation of ACC, without significant increase of AMPK Thr^{172} phosphorylation (Figures S6c-e). The direct involvement of AMPKα2 was confirmed by analyzing myotubes lacking AMPKα2 or both the *α1* and α2 subunits (Lantier et al., 2010). Like in MEFs, FAO was impaired in the α2KO and DKO myotubes. Similarly, the CDK4 inhibitor failed to increase FAO in α2KO and DKO myotubes (Figures 5f and S6f). Rescue of AMPK DKO myotubes with the AMPKα2 S>A mutant triggered ACC phosphorylation levels that where higher than those observed in AMPK α2-transfected cells both in the basal state or upon stimulation with A769662 (Figure 5g). Similarly, ectopic expression of the AMPKα2 S>A mutant in the FAO-defective AMPK DKO myotubes rescued palmitate oxidation to levels similar to those of WT myotubes (Figures 5h and S6g). Taken together, these results in muscle cells confirm that CDK4 modulates FAO through the specific inhibition of AMPKα2 activity, and that a non-phosphorylatable AMPKα2 mutant has a FAO-promoting activity.

CDK4 modulates oxidative metabolism and exercise capacity *in vivo*

We next investigated the contribution of CDK4 to oxidative metabolism and muscle function *in vivo*. Isolated mitochondria from *Cdk4*$^{-/-}$ muscles showed increased oxygen consumption, suggesting increased fatty acid oxidation capacity (Figures 6a-b). Increased FAO was further demonstrated by using intact muscle fibers from Flexor digitorum brevis (FDB) muscle (Figure 6c). Fibers from *Cdk4*$^{-/-}$ FDB muscle metabolized palmitate at a higher rate (Figure 6c-d) and were capable to reach a higher maximal respiration (Figure 6c and 6e). The increased capacity of the muscles of *Cdk4*$^{-/-}$ mice to oxidize fatty acids suggested an overall metabolic phenotype in these mice.

Cdk4$^{-/-}$ mice have decreased body weight (Figure 6f). Consistent with increased AMPK activity, *Cdk4*$^{-/-}$ mice exhibit increased exercise capacity and decreased RER, indicating a preference towards fat oxidation (Figures 6g-i). An 8-day treatment with LY2835219 did not trigger significant alterations in body weight, and food intake (Figures 6j and S7d), although it induced a consistent albeit non-significant decrease in fat mass (Figure S7c) and a modest but significant increase in exercise performance (Figure 6k). A decrease in RER was observed after 4-5 days of treatment (Figure 6l-m). *In vivo*, the inhibition of CDK4 triggered an increase in the phosphorylation of ACC in quadriceps muscle (Figures S7e and S7g), suggesting increased AMPK activity. This was accompanied by an increase of the slow-twitch fiber marker MyHC I (Figure S7i). MyHC I mRNA levels were also increased in gastrocnemius and tibialis muscles from LY2835219 treated animals (Figures S7h-j). Overall, these data suggest that CDK4 is a negative regulator of exercise capacity and whole body oxidative metabolism in mice.

CDK4 regulation of oxidative metabolism and exercise capacity *in vivo* requires muscle AMPK

To determine if the effects of CDK4 inhibition in exercise performance and whole body oxidative metabolism require muscle AMPK, we treated muscle-specific AMPK $\alpha 1/\alpha 2$ KO mice (MDKO) (Lantier et al., 2014) with the CDK4 inhibitor. Consistently, treatment with LY2835219 did not trigger significant alterations in body weight, or food intake (Figures 7a and S7m) in control nor in AMPK MDKO animals. In control animals, LY2835219 was sufficient to trigger a

decrease in fat mass (albeit not significant, p=0.1243), a modest increase in exercise performance and a decrease in RER (Figures 7b-d and S7l). In agreement with previous reports (Lantier et al., 2014; O'Neill et al., 2011), AMPK MDKO animals showed decreased RER and decreased exercise capacity (Figures 7b-d). However, they were not affected by the treatment with LY2835219 under our experimental conditions (Figures 7a-d and S7k-m). Taken together, these results show that the negative effects of CDK4 in oxidative metabolism and exercise performance *in vivo* involve muscle AMPK activity.

Discussion

The contribution of CDK4 to the control of cell cycle progression, via pocket proteins and E2F transcription factors, has been extensively studied (Malumbres, 2014) for more than two decades. However, only recently the CDK4/6-pRB/E2F1 pathway was implicated in metabolic regulation (Aguilar and Fajas, 2010; Blanchet et al., 2011; Denechaud et al., 2016; Lagarrigue et al., 2016; Lee et al., 2014; Lopez-Mejia and Fajas, 2015; Petrov et al., 2016; Salazar-Roa and Malumbres, 2016). Our study provides now evidence that the cell cycle kinase CDK4 is a key player in the control of cellular energy homeostasis, and can also act independently of E2F1 to regulate metabolic pathways.

Three major findings are described here. First, we found that CDK4 negatively regulates the AMPK pathway and, thus, inhibits FAO through phosphorylation of the AMPKα2 subunit. Indeed, *Cdk4*$^{-/-}$ MEFs behaved like cells treated with an AMPK activator and exhibited high FAO levels and low levels of anaerobic glycolysis. Consistently, *Cdk4*$^{R24C/R24C}$ cells exhibited increased anaerobic glycolysis and very low FAO levels. A similar phenotype was observed in AMPK α2KO MEFs. Therefore, CDK4 activity is inversely correlated with AMPKα2-dependent activity. These findings indicate that CDK4 plays a central role in mitochondrial FAO that involves AMPKα2 inhibition and is independent of other downstream effectors, such as E2F1.

Cell division requires high cellular energy levels. Despite the recent evidence that underscore the existence of a crosstalk between cell cycle regulators and energy metabolism (Lopez-Mejia and Fajas, 2015; Salazar-Roa and Malumbres, 2016); the molecular mechanisms coupling energy production and cell cycle

progression remain to be elucidated. Based on our results, we propose that, to exert its role in both cell cycle progression and the insulin signaling pathway, CDK4 represses catabolism by directly targeting at least one of the catalytic subunits of AMPK, namely the α2 subunit. Interestingly, AKT, another key player of the insulin signaling pathway, phosphorylates the α1 subunit of AMPK, thus reducing α1 Thr172 phosphorylation and the subsequent activation of the AMPK heterotrimer (Hawley et al., 2014; Horman et al., 2006a). Remarkably, previous evidence from our laboratory demonstrates that CDK4 is a key effector of the AKT pathway (Lagarrigue et al., 2016). Surprisingly, GSK3 has been reported to inhibit AMPK activity, after phosphorylation of the α subunit by AKT(Suzuki et al., 2013). This finding is somehow unexpected since GSK3 activity is negatively regulated via phosphorylation by AKT, upon insulin stimulation. Moreover, GSK3 is known to inhibit rather than promote anabolic pathways, like the synthesis of glycogen (Cohen and Frame, 2001).

The second major finding in our study is the observation that the function of AMPK heterotrimers can differ depending on their α subunit isoform. Rather few studies have focused on the specific function of each AMPK subunit (although see a recent review (Ross et al., 2016b)), and models completely lacking AMPK activity are often used to study the function of AMPK. Liver-specific deletion or overexpression of the AMPKα2 subunit suggested that this isoform is involved in regulating the balance between lipid synthesis and FAO (Andreelli et al., 2006; Foretz et al., 2005), but these studies did not assess the differences in specificity between α1 and α2. Interestingly, leptin was shown to directly trigger FAO in muscle (Minokoshi et al., 2002), and to trigger an anorexigenic response in hypothalamus (Minokoshi et al., 2004), in an AMPKα2-dependent manner. The effect on food intake may be triggered through AKT signaling via phosphorylation of AMPKα2 by p70S6K (Dagon et al., 2012). Other positive energy balance signals can also reduce food intake via AMPKα2 activity in the brain (Claret et al., 2007; Kim et al., 2004). The isoform-specific roles of AMPK isoforms in whole body energy homeostasis were further highlighted by the fact that the AMPKα2 subunit is essential for nicotine-triggered lipolysis in adipocytes (Wu et al., 2015). However, the specific regulation of energy homeostasis by AMPKα2, and the

molecular mechanisms regulating α2-isoform specific AMPK activity have remained largely unknown.

The third major finding in our study is that the modulation of CDK4 activity *in vivo* can result in modifications in whole body energy homeostasis and exercise performance. These modifications require the expression of AMPK in skeletal muscle. Our results are in agreement with previous studies demonstrating that the use of AICAR can increase exercise performance in sedentary mice while increasing the proportion of slow twitch fibers (Narkar et al., 2008). However, the exact mechanisms that mediate this phenotype remain to be studied. Global approaches to determine muscle reprograming at the proteomics and gene expression level will allow further study of the involvement of CDK4 in muscle biology, and most particularly in exercise. Given that muscle expresses the AMPKα2 subunit highly, and responds to exercise by down-regulating CDK activity (Hoffman et al., 2015), we believe that the study of CDK4-AMPKα2 interaction in skeletal muscle will be highly relevant to the discovery of pharmacological interventions to promote or enhance the beneficial effects of exercise on general health.

By identifying 4 new specific CDK4 phosphosites in the α2 subunit of AMPK, we have discovered a specific role for this subunit in the control of fatty acid metabolism, which we could not demonstrate for the α1 subunit. Interestingly, we detected the phosphorylation of two of these residues, Ser^{377} and Ser^{345}, in muscle samples from resting mice and in myotubes stimulated with insulin or IGF1.

FAO repression by CDK4 emerges as an additional level of metabolic regulation by this kinase, which also mediates other effects of the insulin signaling pathway (Lagarrigue et al., 2016), including lipid synthesis, glycolysis (Denechaud et al., 2016) and proliferation (Malumbres and Barbacid, 2005).

In conclusion, our results demonstrate that CDK4 is a major regulator of cellular energy homeostasis. By combining experimental data from cellular metabolism analyses, biochemistry and molecular biology studies and *in vivo* experiments, our work provides insights into the complex regulation of anabolic and catabolic pathways. These novel findings can have broad implications, not only in the regulation of cell metabolism during proliferation, but also in the control of

energy utilization at the level of the whole organism. Moreover, they highlight the need to delve deeper into the specific functions of the different AMPK heterotrimers, as well as in the regulation of AMPK inactivation.

Author contributions

ICLM and LF designed this study. ICLM guided and performed most experiments, with assistance from SL, AG, LMC, PDD, NZ, CC, BD, JCA, AN, LZ and CC. MO performed HPLC analysis for AMP-ADP-ATP quantification. BV generated the *Prkaa1*$^{-/-}$, *Prkaa2*$^{-/-}$ individual KOs and *Prkaa1*$^{-/-}$; *Prkaa2*$^{-/-}$ double KO MEF cells and myoblasts, as well as the muscle specific *Prkaa1*$^{-/-}$; *Prkaa2*$^{-/-}$ double KO mice. DGH helped to design the experiments and provided AMPK constructs. ICLM and LF wrote the manuscript.

Acknowledgements

We acknowledge all of the members of the Fajas laboratory for support and discussions. We thank P. Waridel and M. Quadroni from the Protein Analysis Facility, Center for Integrative Genomics, Faculty of Biology and Medecine, University of Lausanne, Switzerland for their help with mass spectrometry analysis.

We thank M. Barbacid for providing the *Cdk4*$^{R24C/R24C}$ and *Cdk4*$^{-/-}$ mice that were used to prepare MEFs. This work was supported by the Swiss National Science Foundation.

References

Aguilar, V., and Fajas, L. (2010). Cycling through metabolism. EMBO Mol Med *2*, 338-348.

Andreelli, F., Foretz, M., Knauf, C., Cani, P.D., Perrin, C., Iglesias, M.A., Pillot, B., Bado, A., Tronche, F., Mithieux, G.*, et al.* (2006). Liver adenosine monophosphate-activated kinase-alpha2 catalytic subunit is a key target for the control of hepatic glucose production by adiponectin and leptin but not insulin. Endocrinology *147*, 2432-2441.

Blanchet, E., Annicotte, J.S., Lagarrigue, S., Aguilar, V., Clape, C., Chavey, C., Fritz, V., Casas, F., Apparailly, F., Auwerx, J.*, et al.* (2011). E2F transcription factor-1 regulates oxidative metabolism. Nat Cell Biol *13*, 1146-1152.

Carling, D. (2004). Ampk. Curr Biol *14*, R220.

Claret, M., Smith, M.A., Batterham, R.L., Selman, C., Choudhury, A.I., Fryer, L.G., Clements, M., Al-Qassab, H., Heffron, H., Xu, A.W.*, et al.* (2007). AMPK is essential

for energy homeostasis regulation and glucose sensing by POMC and AgRP neurons. J Clin Invest *117*, 2325-2336.
Cohen, P., and Frame, S. (2001). The renaissance of GSK3. Nat Rev Mol Cell Biol *2*, 769-776.
Dagon, Y., Hur, E., Zheng, B., Wellenstein, K., Cantley, L.C., and Kahn, B.B. (2012). p70S6 kinase phosphorylates AMPK on serine 491 to mediate leptin's effect on food intake. Cell Metab *16*, 104-112.
Daub, H., Olsen, J.V., Bairlein, M., Gnad, F., Oppermann, F.S., Korner, R., Greff, Z., Keri, G., Stemmann, O., and Mann, M. (2008). Kinase-selective enrichment enables quantitative phosphoproteomics of the kinome across the cell cycle. Mol Cell *31*, 438-448.
Denechaud, P.D., Lopez-Mejia, I.C., Giralt, A., Lai, Q., Blanchet, E., Delacuisine, B., Nicolay, B.N., Dyson, N.J., Bonner, C., Pattou, F.*, et al.* (2016). E2F1 mediates sustained lipogenesis and contributes to hepatic steatosis. J Clin Invest *126*, 137-150.
Dinkel, H., Chica, C., Via, A., Gould, C.M., Jensen, L.J., Gibson, T.J., and Diella, F. (2011). Phospho.ELM: a database of phosphorylation sites--update 2011. Nucleic Acids Res *39*, D261-267.
Djouder, N., Tuerk, R.D., Suter, M., Salvioni, P., Thali, R.F., Scholz, R., Vaahtomeri, K., Auchli, Y., Rechsteiner, H., Brunisholz, R.A.*, et al.* (2010). PKA phosphorylates and inactivates AMPKalpha to promote efficient lipolysis. EMBO J *29*, 469-481.
Foretz, M., Ancellin, N., Andreelli, F., Saintillan, Y., Grondin, P., Kahn, A., Thorens, B., Vaulont, S., and Viollet, B. (2005). Short-term overexpression of a constitutively active form of AMP-activated protein kinase in the liver leads to mild hypoglycemia and fatty liver. Diabetes *54*, 1331-1339.
Fullerton, M.D., Galic, S., Marcinko, K., Sikkema, S., Pulinilkunnil, T., Chen, Z.P., O'Neill, H.M., Ford, R.J., Palanivel, R., O'Brien, M.*, et al.* (2013). Single phosphorylation sites in Acc1 and Acc2 regulate lipid homeostasis and the insulin-sensitizing effects of metformin. Nat Med *19*, 1649-1654.
Gnad, F., Gunawardena, J., and Mann, M. (2011). PHOSIDA 2011: the posttranslational modification database. Nucleic Acids Res *39*, D253-260.
Goransson, O., McBride, A., Hawley, S.A., Ross, F.A., Shpiro, N., Foretz, M., Viollet, B., Hardie, D.G., and Sakamoto, K. (2007). Mechanism of action of A-769662, a valuable tool for activation of AMP-activated protein kinase. J Biol Chem *282*, 32549-32560.
Grahame Hardie, D. (2016). Regulation of AMP-activated protein kinase by natural and synthetic activators. Acta Pharm Sin B *6*, 1-19.
Hardie, D.G. (2015). AMPK: positive and negative regulation, and its role in whole-body energy homeostasis. Curr Opin Cell Biol *33*, 1-7.
Hardie, D.G., and Pan, D.A. (2002). Regulation of fatty acid synthesis and oxidation by the AMP-activated protein kinase. Biochem Soc Trans *30*, 1064-1070.
Hardie, D.G., Ross, F.A., and Hawley, S.A. (2012). AMPK: a nutrient and energy sensor that maintains energy homeostasis. Nat Rev Mol Cell Biol *13*, 251-262.
Hawley, S.A., Boudeau, J., Reid, J.L., Mustard, K.J., Udd, L., Makela, T.P., Alessi, D.R., and Hardie, D.G. (2003). Complexes between the LKB1 tumor suppressor, STRADa/b and MO25a/b are upstream kinases in the AMP-activated protein kinase cascade. J. Biol. *2*, 28.
Hawley, S.A., Davison, M., Woods, A., Davies, S.P., Beri, R.K., Carling, D., and Hardie, D.G. (1996). Characterization of the AMP-activated protein kinase kinase from rat

liver and identification of threonine 172 as the major site at which it phosphorylates AMP-activated protein kinase. J Biol Chem *271*, 27879-27887.
Hawley, S.A., Pan, D.A., Mustard, K.J., Ross, L., Bain, J., Edelman, A.M., Frenguelli, B.G., and Hardie, D.G. (2005). Calmodulin-dependent protein kinase kinase-beta is an alternative upstream kinase for AMP-activated protein kinase. Cell Metab. *2*, 9-19.
Hawley, S.A., Ross, F.A., Gowans, G.J., Tibarewal, P., Leslie, N.R., and Hardie, D.G. (2014). Phosphorylation by Akt within the ST loop of AMPK-alpha1 down-regulates its activation in tumour cells. Biochem J *459*, 275-287.
Hoffman, N.J., Parker, B.L., Chaudhuri, R., Fisher-Wellman, K.H., Kleinert, M., Humphrey, S.J., Yang, P., Holliday, M., Trefely, S., Fazakerley, D.J., *et al.* (2015). Global Phosphoproteomic Analysis of Human Skeletal Muscle Reveals a Network of Exercise-Regulated Kinases and AMPK Substrates. Cell Metab *22*, 922-935.
Horman, S., Vertommen, D., Heath, R., Neumann, D., Mouton, V., Woods, A., Schlattner, U., Wallimann, T., Carling, D., Hue, L., *et al.* (2006a). Insulin antagonizes ischemia-induced Thr172 phosphorylation of AMP-activated protein kinase alpha-subunits in heart via hierarchical phosphorylation of Ser485/491. J Biol Chem *281*, 5335-5340.
Horman, S., Vertommen, D., Heath, R., Neumann, D., Mouton, V., Woods, A., Schlattner, U., Wallimann, T., Carling, D., Hue, L., *et al.* (2006b). Insulin antagonizes ischemia-induced Thr172 phosphorylation of AMP-activated protein kinase alpha-subunits in heart via hierarchical phosphorylation of Ser485/491. J. Biol. Chem. *281*, 5335-5340.
Hornbeck, P.V., Zhang, B., Murray, B., Kornhauser, J.M., Latham, V., and Skrzypek, E. (2015). PhosphoSitePlus, 2014: mutations, PTMs and recalibrations. Nucleic Acids Res *43*, D512-520.
Humphrey, S.J., Azimifar, S.B., and Mann, M. (2015). High-throughput phosphoproteomics reveals in vivo insulin signaling dynamics. Nat Biotechnol *33*, 990-995.
Hurley, R.L., Anderson, K.A., Franzone, J.M., Kemp, B.E., Means, A.R., and Witters, L.A. (2005). The Ca^{2+}/calmoldulin-dependent protein kinase kinases are AMP-activated protein kinase kinases. J. Biol. Chem. *280*, 29060-29066.
Hurley, R.L., Barre, L.K., Wood, S.D., Anderson, K.A., Kemp, B.E., Means, A.R., and Witters, L.A. (2006). Regulation of AMP-activated protein kinase by multisite phosphorylation in response to agents that elevate cellular cAMP. J Biol Chem *281*, 36662-36672.
Icreverzi, A., de la Cruz, A.F., Van Voorhies, W.A., and Edgar, B.A. (2012). Drosophila cyclin D/Cdk4 regulates mitochondrial biogenesis and aging and sensitizes animals to hypoxic stress. Cell Cycle *11*, 554-568.
Jones, R.G., and Thompson, C.B. (2009). Tumor suppressors and cell metabolism: a recipe for cancer growth. Genes Dev *23*, 537-548.
Kettenbach, A.N., Schweppe, D.K., Faherty, B.K., Pechenick, D., Pletnev, A.A., and Gerber, S.A. (2011). Quantitative phosphoproteomics identifies substrates and functional modules of Aurora and Polo-like kinase activities in mitotic cells. Sci Signal *4*, rs5.
Kim, M.S., Park, J.Y., Namkoong, C., Jang, P.G., Ryu, J.W., Song, H.S., Yun, J.Y., Namgoong, I.S., Ha, J., Park, I.S., *et al.* (2004). Anti-obesity effects of alpha-lipoic acid mediated by suppression of hypothalamic AMP-activated protein kinase. Nat Med *10*, 727-733.

Laderoute, K.R., Amin, K., Calaoagan, J.M., Knapp, M., Le, T., Orduna, J., Foretz, M., and Viollet, B. (2006). 5'-AMP-activated protein kinase (AMPK) is induced by low-oxygen and glucose deprivation conditions found in solid-tumor microenvironments. Mol Cell Biol *26*, 5336-5347.

Lagarrigue, S., Lopez-Mejia, I.C., Denechaud, P.D., Escote, X., Castillo-Armengol, J., Jimenez, V., Chavey, C., Giralt, A., Lai, Q., Zhang, L.*, et al.* (2016). CDK4 is an essential insulin effector in adipocytes. J Clin Invest *126*, 335-348.

Lantier, L., Fentz, J., Mounier, R., Leclerc, J., Treebak, J.T., Pehmoller, C., Sanz, N., Sakakibara, I., Saint-Amand, E., Rimbaud, S.*, et al.* (2014). AMPK controls exercise endurance, mitochondrial oxidative capacity, and skeletal muscle integrity. FASEB J *28*, 3211-3224.

Lantier, L., Mounier, R., Leclerc, J., Pende, M., Foretz, M., and Viollet, B. (2010). Coordinated maintenance of muscle cell size control by AMP-activated protein kinase. FASEB J *24*, 3555-3561.

Lee, Y., Dominy, J.E., Choi, Y.J., Jurczak, M., Tolliday, N., Camporez, J.P., Chim, H., Lim, J.H., Ruan, H.B., Yang, X.*, et al.* (2014). Cyclin D1-Cdk4 controls glucose metabolism independently of cell cycle progression. Nature *510*, 547-551.

Lopez-Cotarelo, P., Escribano-Diaz, C., Gonzalez-Bethencourt, I.L., Gomez-Moreira, C., Deguiz, M.L., Torres-Bacete, J., Gomez-Cabanas, L., Fernandez-Barrera, J., Delgado-Martin, C., Mellado, M.*, et al.* (2015). A novel MEK-ERK-AMPK signaling axis controls chemokine receptor CCR7-dependent survival in human mature dendritic cells. J Biol Chem *290*, 827-840.

Lopez-Mejia, I.C., and Fajas, L. (2015). Cell cycle regulation of mitochondrial function. Curr Opin Cell Biol *33*, 19-25.

Malumbres, M. (2014). Cyclin-dependent kinases. Genome Biol *15*, 122.

Malumbres, M., and Barbacid, M. (2001). To cycle or not to cycle: a critical decision in cancer. Nat Rev Cancer *1*, 222-231.

Malumbres, M., and Barbacid, M. (2005). Mammalian cyclin-dependent kinases. Trends Biochem Sci *30*, 630-641.

Malumbres, M., and Barbacid, M. (2009). Cell cycle, CDKs and cancer: a changing paradigm. Nat Rev Cancer *9*, 153-166.

Manfredi, G., Yang, L., Gajewski, C.D., and Mattiazzi, M. (2002). Measurements of ATP in mammalian cells. Methods *26*, 317-326.

Martin Campos, T., Mylonas, R., Masselot, A., Waridel, P., Petricevic, T., Xenarios, I., and Quadroni, M. (2017). MsViz, a graphical software tool for in-depth manual validation and quantitation of post-translational modifications. J Proteome Res.

Minokoshi, Y., Alquier, T., Furukawa, N., Kim, Y.B., Lee, A., Xue, B., Mu, J., Foufelle, F., Ferre, P., Birnbaum, M.J.*, et al.* (2004). AMP-kinase regulates food intake by responding to hormonal and nutrient signals in the hypothalamus. Nature *428*, 569-574.

Minokoshi, Y., Kim, Y.B., Peroni, O.D., Fryer, L.G., Muller, C., Carling, D., and Kahn, B.B. (2002). Leptin stimulates fatty-acid oxidation by activating AMP-activated protein kinase. Nature *415*, 339-343.

Moreno, D., Knecht, E., Viollet, B., and Sanz, P. (2008). A769662, a novel activator of AMP-activated protein kinase, inhibits non-proteolytic components of the 26S proteasome by an AMPK-independent mechanism. FEBS Lett *582*, 2650-2654.

Morizane, Y., Thanos, A., Takeuchi, K., Murakami, Y., Kayama, M., Trichonas, G., Miller, J., Foretz, M., Viollet, B., and Vavvas, D.G. (2011). AMP-activated protein

kinase suppresses matrix metalloproteinase-9 expression in mouse embryonic fibroblasts. J Biol Chem *286*, 16030-16038.
Mounier, R., Theret, M., Lantier, L., Foretz, M., and Viollet, B. (2015). Expanding roles for AMPK in skeletal muscle plasticity. Trends Endocrinol Metab *26*, 275-286.
Narkar, V.A., Downes, M., Yu, R.T., Embler, E., Wang, Y.X., Banayo, E., Mihaylova, M.M., Nelson, M.C., Zou, Y., Juguilon, H.*, et al.* (2008). AMPK and PPARdelta agonists are exercise mimetics. Cell *134*, 405-415.
O'Leary, B., Finn, R.S., and Turner, N.C. (2016). Treating cancer with selective CDK4/6 inhibitors. Nat Rev Clin Oncol *13*, 417-430.
O'Neill, H.M., Lally, J.S., Galic, S., Thomas, M., Azizi, P.D., Fullerton, M.D., Smith, B.K., Pulinilkunnil, T., Chen, Z., Samaan, M.C.*, et al.* (2014). AMPK phosphorylation of ACC2 is required for skeletal muscle fatty acid oxidation and insulin sensitivity in mice. Diabetologia *57*, 1693-1702.
O'Neill, H.M., Maarbjerg, S.J., Crane, J.D., Jeppesen, J., Jorgensen, S.B., Schertzer, J.D., Shyroka, O., Kiens, B., van Denderen, B.J., Tarnopolsky, M.A.*, et al.* (2011). AMP-activated protein kinase (AMPK) beta1beta2 muscle null mice reveal an essential role for AMPK in maintaining mitochondrial content and glucose uptake during exercise. Proc Natl Acad Sci U S A *108*, 16092-16097.
Petrov, P.D., Ribot, J., Lopez-Mejia, I.C., Fajas, L., Palou, A., and Bonet, M.L. (2016). Retinoblastoma Protein Knockdown Favors Oxidative Metabolism and Glucose and Fatty Acid Disposal in Muscle Cells. J Cell Physiol *231*, 708-718.
Rane, S.G., Cosenza, S.C., Mettus, R.V., and Reddy, E.P. (2002). Germ line transmission of the Cdk4(R24C) mutation facilitates tumorigenesis and escape from cellular senescence. Mol Cell Biol *22*, 644-656.
Rane, S.G., Dubus, P., Mettus, R.V., Galbreath, E.J., Boden, G., Reddy, E.P., and Barbacid, M. (1999). Loss of Cdk4 expression causes insulin-deficient diabetes and Cdk4 activation results in beta-islet cell hyperplasia. Nat Genet *22*, 44-52.
Ross, F.A., Jensen, T.E., and Hardie, D.G. (2016a). Differential regulation by AMP and ADP of AMPK complexes containing different gamma subunit isoforms. Biochem. J. *473*, 189-199.
Ross, F.A., MacKintosh, C., and Hardie, D.G. (2016b). AMP-activated protein kinase: a cellular energy sensor that comes in 12 flavours. FEBS J. *283*, 2987-3001.
Salazar-Roa, M., and Malumbres, M. (2016). Fueling the Cell Division Cycle. Trends Cell Biol.
Schindelin, J., Arganda-Carreras, I., Frise, E., Kaynig, V., Longair, M., Pietzsch, T., Preibisch, S., Rueden, C., Saalfeld, S., Schmid, B.*, et al.* (2012). Fiji: an open-source platform for biological-image analysis. Nat Methods *9*, 676-682.
Shaw, R.J., Kosmatka, M., Bardeesy, N., Hurley, R.L., Witters, L.A., DePinho, R.A., and Cantley, L.C. (2004). The tumor suppressor LKB1 kinase directly activates AMP-activated kinase and regulates apoptosis in response to energy stress. Proc. Natl. Acad. Sci. USA *101*, 3329-3335.
Suzuki, T., Bridges, D., Nakada, D., Skiniotis, G., Morrison, S.J., Lin, J.D., Saltiel, A.R., and Inoki, K. (2013). Inhibition of AMPK catabolic action by GSK3. Mol Cell *50*, 407-419.
Wolfel, T., Hauer, M., Schneider, J., Serrano, M., Wolfel, C., Klehmann-Hieb, E., De Plaen, E., Hankeln, T., Meyer zum Buschenfelde, K.H., and Beach, D. (1995). A p16INK4a-insensitive CDK4 mutant targeted by cytolytic T lymphocytes in a human melanoma. Science *269*, 1281-1284.

Woods, A., Dickerson, K., Heath, R., Hong, S.P., Momcilovic, M., Johnstone, S.R., Carlson, M., and Carling, D. (2005). Ca2+/calmodulin-dependent protein kinase kinase-beta acts upstream of AMP-activated protein kinase in mammalian cells. Cell Metab. *2*, 21-33.
Woods, A., Johnstone, S.R., Dickerson, K., Leiper, F.C., Fryer, L.G., Neumann, D., Schlattner, U., Wallimann, T., Carlson, M., and Carling, D. (2003). LKB1 is the upstream kinase in the AMP-activated protein kinase cascade. Curr. Biol. *13*, 2004-2008.
Wu, Y., Song, P., Zhang, W., Liu, J., Dai, X., Liu, Z., Lu, Q., Ouyang, C., Xie, Z., Zhao, Z., *et al.* (2015). Activation of AMPKalpha2 in adipocytes is essential for nicotine-induced insulin resistance in vivo. Nat Med *21*, 373-382.
Zhang, C.S., Hawley, S.A., Zong, Y., Li, M.Q., Wang, Z.C., Gray, A., Ma, T., Cui, J.W., Feng, J.W., Zhu, M.J., *et al.* (2017). FBP aldolases are glucose sensors controlling AMPK activation. Nature, in press.

FIGURE LEGENDS

Figure 1. CDK4 modulates FAO in an E2F1-independent manner

Cdk4$^{+/+}$, *Cdk4*$^{-/-}$ and *Cdk4*$^{R24C/R24C}$ MEFs were submitted to a glycolysis assay, during which ECAR was measured at the basal level and upon glucose injection (a), or to a FAO assay, in which the palmitate induced OCR was measured (in % OCR compared to the basal OCR) (c). The glycolytic rate was calculated in (b). The area under curve of the palmitate induced OCR was quantified in (d).

E2f1$^{+/+}$, *E2f1*$^{-/-}$, *Cdk4*$^{R24C/R24C}$ *E2f1*$^{+/+}$ and *Cdk4*$^{R24C/R24C}$ *E2f1*$^{-/-}$ MEFs were submitted to a glycolysis assay, during which ECAR was measured at the basal level and upon glucose injection (e), or to a FAO assay, in which the palmitate induced OCR was measured (in % OCR compared to the basal OCR) (g). The glycolytic rate was calculated in (f). The area under curve of the palmitate induced OCR was quantified in (h).

Data were expressed as mean ± s.e.m.

Figure 2. CDK4 regulation of FAO is AMPK-dependent

Cdk4$^{+/+}$, *Cdk4*$^{-/-}$ and *Cdk4*$^{R24C/R24C}$ MEFs were starved for 3 hours and then stimulated with 50μM A769662, the western blot analysis shows the A769662 induced ACC phosphorylation in *Cdk4*$^{+/+}$, *Cdk4*$^{-/-}$ and *Cdk4*$^{R24C/R24C}$ cells (a). The pACC levels were quantified in (b). SV40 immortalized cells were placed in KHB medium containing 1.5mM carnitine and 300μM Oleate for AMP, ADP and ATP

quantification by HPLC. The AMP/ATP and ADP/ATP ratios are shown in (c) and (d). The AMP/ATP and ADP/ATP ratios of WT SV40 immortalized cells treated with 50µM A769662 for 8 hours are shown in (e) and (f). *Cdk4*$^{+/+}$, *Cdk4*$^{-/-}$ and *Cdk4*$^{R24C/R24C}$ MEFs were treated with DMSO or 50µM A769662 for 2 hours in KHB medium and submitted to a FAO assay in which the palmitate induced OCR was measured (in % OCR compared to the basal OCR). The area under curve of the palmitate induced OCR was quantified in (g).

Data were expressed as mean ± s.e.m. See also Figure S1.

Figure 3. The AMPKα2 subunit is required for efficient fatty acid oxidation in MEFs

AMPK WT, AMPK A1 KO, AMPK A2 KO and AMPK DKO SV40-immortalized MEFs were submitted to a glycolysis assay, during which ECAR was measured at the basal level and upon glucose injection (a), or to a FAO assay, in which the palmitate induced OCR was measured (in % OCR compared to the basal OCR) (c). The glycolytic rate was calculated in (b). The area under curve of the palmitate induced OCR was quantified in (d).

AMPK WT and AMPK A2 KO SV40-immortalized MEFs were treated for 2 hours with DMSO or 50µM A769662 for 2 hours in KHB medium and submitted to a FAO assay in which the palmitate induced OCR was measured (in % OCR compared to the basal OCR) (e). The area under curve of the palmitate induced OCR was quantified in (f).

Data were expressed as mean ± s.e.m. See also Figure S2.

Figure 4. CDK4 phosphorylates the AMPK*α*2 subunit

(a) Cyclin D3-CDK4 directly phosphorylates full-length GST-AMPK subunits *in vitro* (n=3). Asterisks mark the proteins of interest. The Phosphorylation score (in % of RB phosphorylation) was determined in (b). CDK consensus sites in human AMPKα2 *(PRKAA2*) are depicted in (c). (d) *In vitro* phosphorylation of WT and mutated (Ser or Thr to Ala) GST-AMPK α2 fragments (D1: 1-245 aa, D2: 246-356 aa, D3: 357-422 aa, D4: 432-522 and D2-3: 246-422 aa, 1100-1321aa) by Cyclin D3/CDK4 (n=3). The Phosphorylation score (in % of the WT fragment) was determined in (e). (f) *In vitro* phosphorylation of full-length WT GST-AMPKα2 and

full-length S>A GST-AMPKα2 by Cyclin D3/CDK4 (n=3). The Phosphorylation score (in % of RB phosphorylation) was determined in (g). Kinase dead AMPK α2β2γ1 trimers were used as a substrate for Cyclin D3-CDK4 complex and analyzed by mass spectrometry. A graphical overview of the sequence coverage of AMPKα2 human protein in samples displayed by MsViz is depicted in (h). The thickness of the green bars is a function of the number of spectra matching the sequence region, while modification sites are labeled and shown as circles with size proportional to the number of spectra matching a given position.

A truncated form of RB (hRB 379-928aa) was used as a positive control. A representative autoradiography for each kinase assay is shown.

See also Figure S3.

Figure 5. AMPK*α*2 phosphorylation is necessary and sufficient for FAO repression by CDK4

AMPK DKO SV40-immortalized MEFs were electroporated with plasmids encoding Myc-tagged AMPK A1, Myc-tagged AMPK A2 and Myc-tagged AMPK A2 S>A. 48h after, MEFs were starved for 3 hours, and treated for 2 hours with DMSO or 50μM A769662 before protein extraction, the western blot analysis shows the A769662 induced ACC phosphorylation in transfected cells (a).

Electroporated MEFs were submitted to a FAO assay 48h after transfection, in which the palmitate induced OCR was measured (in % OCR compared to the basal OCR). The area under curve of the palmitate induced OCR was quantified in (b).

AMPK WT and AMPK DKO SV40-immortalized MEFs were treated with DMSO or LY2835219 1,5μM for 24h, and submitted to a FAO assay, in which the palmitate induced OCR was measured (in % OCR compared to the basal OCR). The area under curve of the palmitate induced OCR was quantified in (c).

AMPK WT SV40 immortalized cells were treated for 8h with DMSO or LY2835219 1,5μM. AMP, ADP and ATP were quantified by HPLC. The AMP/ATP and ADP/ATP ratios are shown in (d) and (e).

AMPK DKO myotubes were transfected with plasmids encoding Myc-tagged AMPK A2 and Myc-tagged AMPK A2 S>A. B. 48h after, myotubes were treated for 2 hours with DMSO or 50μM A769662 before protein extraction, the western blot analysis shows the A769662 induced ACC phosphorylation in transfected cells (g). Transfected myotubes were submitted to a FAO assay in which the palmitate

induced OCR was measured (in % OCR compared to the basal OCR). The area under curve of the palmitate induced OCR was quantified in (h).
Data were expressed as mean ± s.e.m. See also Figure S4 and S5.

Figure 6. CDK4 modulates oxidative metabolism and exercise capacity *in vivo*

Mitochondria isolated from gastrocnemius (a) and quadriceps (b) muscle from *Cdk4*$^{+/+}$ and *Cdk4*$^{-/-}$ mice were submitted to a respiration assay using fatty acids as a substrate. Isolated FDB muscle fibers from *Cdk4*$^{+/+}$ and *Cdk4*$^{-/-}$ mice were submitted to a FAO assay in which the palmitate induced OCR was measured (in % OCR compared to the basal OCR) (c). The area under curve of the palmitate induced OCR is shown in (d). The maximal respiration was induced by FCCP and is shown in (e).
Body weight of 25-30 weeks old male *Cdk4*$^{+/+}$ and *Cdk4*$^{-/-}$ mice was measured in (f). *Cdk4*$^{+/+}$ and *Cdk4*$^{-/-}$ were submitted to an exercise capacity testing on treadmill. The time before exhaustion was recorded in (g). RER of the aforementioned mice is depicted in (h) and (i).
30-week-old wild type mice were gavaged with 37mg/kg of LY2835219 or vehicle for 8 days. Body weight (j) and exercise capacity (k) were measured the day after the last treatment. RER of the aforementioned mice after 5 days of treatment is depicted in (l) and (m).
Data were expressed as mean ± s.e.m. See also Figure S6.

Figure 7. CDK4 regulation of oxidative metabolism and exercise capacity *in vivo* requires muscle AMPK

Body weight of 12-16 weeks old AMPK WT and AMPK MDKO females gavaged with 37mg/kg of LY2835219 or vehicle for 8 days was measured in (a). Exercise capacity testing on treadmill. The time before exhaustion was recorded in (b). RER of the aforementioned mice is depicted in (c) and (d).
Data were expressed as mean ± s.e.m. See also Figure S7.

STAR Methods

CONTACT FOR REAGENT AND RESOURCE SHARING

Further information and requests for resources and reagents should be directed to and will fulfilled by Lluis Fajas (lluis.fajas@unil.ch)

EXPERIMENTAL MODEL AND SUBJECT DETAILS

Cell culture

MEFs were derived from embryos that were dissected 13.5 days after vaginal plugs. The *Cdk4*$^{-/-}$ (*Cdk4*^{nc}), *Cdk4*$^{R24C/R24C}$ and *E2f1*$^{-/-}$ mice have been previously described(Denechaud et al., 2016; Lagarrigue et al., 2016).

Prkaa1$^{-/-}$, *Prkaa2*$^{-/-}$ individual KOs; and *Prkaa1*$^{-/-}$; *Prkaa2*$^{-/-}$ double KO SV40 immortalized MEF cells were prepared as described (Laderoute et al., 2006). They are referred in the manuscript as AMPK α1KO, AMPK α2KO and AMPK DKO.

MEFs were cultured in DMEM/F12 supplemented with 10% fetal bovine serum (FBS, PAA Laboratories), glutamax (1mM), sodium pyruvate (1mM), non-essential amino-acids, 2-Mercapto-ethanol (50µM) and antibiotics in 5% CO_2 37°C incubator.

C2C12 myoblasts were obtained from ATCC and were cultured in low-glucose DMEM with 10% FBS in 5% CO_2 37°C incubator. For myotube differentiation, when the cells reached 80-90% confluency, the culture medium was switched to DMEM containing 2% horse serum. The medium was changed every 2 days until day 5 to 7 of differentiation.

Primary myoblasts were grown in collagen coated plates cultured DMEM/F12 supplemented with 20% fetal bovine serum, 2mM Glutamine and FGF (5ng/ml) in 5% CO_2 37°C incubator. For myotube differentiation, cells were plated on matrigel-coated plates when the cells reached 80-90% confluency, the culture medium was switched to DMEM/F12 supplemented with 2% horse serum and 2mM Glutamine. The medium was changed every 2 days until day 4-5 of differentiation. For rescue experiments, myotubes were transfected using lipofectamine 3000 (Thermo Fisher Scientific), at day 1 and day 3 of differentiation. The cells were assayed 48 hours after the 2nd round of transfection.

Primary *Cdk4*$^{+/+}$, *Cdk4*$^{-/-}$ and *Cdk4*$^{R24C/R24C}$ MEFs, as well as primary *E2f1*$^{+/+}$, *E2f1*$^{-/-}$, *Cdk4*$^{R24C/R24C}$ *E2f1*$^{+/+}$ and *Cdk4*$^{R24C/R24C}$ *E2f1*$^{-/-}$ MEFs, between P2 and P5, were used for figures 1 and 2. SV40 immortalized MEFs were used for all other figures.

Animal studies

The generation of *Cdk4*$^{-/-}$, that lack CDK4 in all tissues except pancreatic beta cells and were referred as *Cdk4*$^{nc/nc}$ in our previous study, was described in (Lagarrigue et al., 2016). Male mice were used.

For gavage experiments, C57BL/6J male mice were obtained from Janvier Labs. Animals were gavaged daily with 37mg/kg of LY2835219 or vehicle for 8 days. Mice were acclimated and submitted to indirect calorimetry between day 4 and day 6. Exercise capacity testing was performed the day after the last gavage. Body weight was controlled daily. Food intake was measured in the metabolic cages.

To obtain skeletal muscle AMPK-deficient mice [AMPK_1fl/fl _2fl/fl human skeletal actin (HSA)-Cre_ mice on a C57Bl6- 129Sv mixed background], AMPK_1$^{fl/fl}$_2$^{fl/fl}$ mice were interbred with transgenic mice expressing Cre recombinase under the control of the HSA promoter. Female mice were used.

The mice were housed in a facility on a 12-h light-dark cycle with free access to standard rodent chow and water.

Mice were familiarized to the motorized rodent treadmill (Columbus Instruments, Columbus OH) on the J-2 and J-1 before the evaluation of exercise capacity. Familiarization consisted of an initial 10 min period where the treadmill speed and incline were set to zero with a slight electric shock grid at the back of the carpet set to 20 V, 0.34 mA, and 2 Hz. The treadmill speed was then increased steadily to 10 m/min (J-2) and 12 m/min (J-1) for an additional 10 min.

The day immediately following familiarization to the treadmill, mice were subjected to an exercise capacity test. For this, the mice were acclimated to the treadmill for 10 min, with the speed and incline set initially to zero. The treadmill speed was then increase to 8.5 m/min with an angle of inclination set to 0° for 9 min. Next, the treadmill speed and incline was increased to 10 m/min and 5°, respectively, for 3 min. The speed was then increased by 2.5 m/min every 3 min to a maximum speed of 40 m/min, while inclination was increased by 5° every 9 min

until a maximum incline of 15°.

Strict a priori criteria for exercise-induced exhaustion consisted in: (1) 10 consecutive seconds on the electric grid; (2) spending more than 50% of time on the grid; and/or (3) lack of motivation to manual prodding. Mice were immediately removed from their respective lane once one or more of these criteria were reached.

Following the protocol, mice were killed by cervical dislocation and skeletal muscles were isolated for analysis.

All animal care and treatment procedures were performed in accordance with Swiss guidelines and were approved by the Canton of Vaud, Service de la Consommation et des Affaires Vétérinaires (SCAV) (authorization VD 3121.a).

METHOD DETAILS

Materials

All cell culture reagents were purchased from GIBCO (Thermo Fisher Scientific). All chemicals, except if stated otherwise, were purchased from Sigma-Aldrich. The CDK4 *inhibitor (LY2835219) and* Compound C. were purchased from MedChem Express. Experiments were done using 1μM of LY2835219, unless stated otherwise. The AMPK allosteric activator was purchased from Abcam or MedChem Express. Unless stated otherwise, A769662 was used at a concentration of 50μM. γ□^{33}P-ATP was purchased from Perkin Elmer.

Immunoblot

For western blot analysis, the cells were seeded in 6-well plates 48 hours before the experiment, serum starved for 3 hours, and treated with either LY2835219 or A769662 for 2 hours.

Total proteins extracts were subjected to SDS-PAGE analysis and transferred to nitrocellulose membranes for immunoblotting. The following antibodies were obtained from Cell Signaling Technology : ACC (no. 3662), phosphorylated ACC (ser79) (no. 3661), AMPK (no.2532), phosphorylated AMPK (Thr172) (no 2535), Myc-tag (no. 2276), phosphorylated RB (Ser780) (no. 8180). The following antibodies were obtained from Santa Cruz Technology: Cdk4 (C-22; sc-260), Rb (C-

2; sc-74562), AMPK α2 (sc-19131). A second Myc-tag antibody was used to analyse myotube samples (abcam ab9106)

The α Tubulin (no. T6199) antibody was obtained from Sigma Aldrich, the actin (sc-1615) was obtained from Santa Cruz Technology.

The levels of total proteins and the levels of phosphorylation of proteins were analyzed on separate gels. The band intensities on developed films, fusion FX images or chemidoc images or were quantified using Fiji image processing package (Schindelin et al., 2012).

Plasmid constructs and mutagenesis

pDONR223-hPRKAA1 (ref:23871), pDONR223-hPRKAA2 (ref:23671), pDONR223-hPRKAB1 (ref:23360), pDONR223-hPRKAB2 (ref:23647), pDONR223-hPRKAG1 (ref:23718), pDONR223-hPRKAG2 (ref:23689), pDONR223-hPRKAG3 (ref:23549) were provided from Addgene. The different GST subunits of human AMPK were obtained using the pDEST pGEX-2T vector of Gateway Cloning Technology (Invitrogen) starting from previously described pDONR223AMPK constructs. The different serine-to-alanine mutants of GST-hPRKAA2 were generated using a Quick-Change Site-Directed Mutagenesis kit (Stratagene) with the following primers (Supplemental Table 2). A similar strategy was used to obtain the truncated versions of GST-hPRKAA2 and the different serine-to-alanine mutants using the following primers (Supplemental Table 2).

The Myc-hPRKAA1, the Myc-hPRKAA2 and the Myc-hPRKAA2-S345A-S377A-T485A-S529A were obtained using the pDEST pCDNA3 MYC vector previously and the above described pDONR223-human AMPK constructs. pDONR-hRB 379-928aa was subcloned from pCMV human RB and generated using the pDONR221 vector of Gateway Cloning Technology. The pGEX-2T hRB 379-928aa was obtained using the pDEST pGEX-2T from Gateway Cloning Technology.

GST production

Independent AMPK subunits were cloned in the pDEST pGEX-2T and expressed in BL21 bacteria. GST-purified proteins were re-suspended in 50mM Tris.HCl [pH 8], 100 mM NaCl, 5 mM DTT and 20% glycerol buffer.

CDK4 Kinase assay

Kinase assays were performed using Independent AMPK subunits proteins and 500ng of recombinant RB protein (Santa Cruz) as a substrate in kinase buffer (25 mM Tris.HCl [pH 7.5], 150 mM NaCl, 10 mM $MgCl_2$, 1 mM DTT, 5 mM $Na_4P_2O_7$, 50 mM NaF, 1 mM vanadate and protease inhibitor cocktail) with 40 µM ATP and 8 µCi γ□^{33P}ATP (Perkin Elmer) for 30 min at 30°C. Recombinant CDK4/cyclin D3 kinase and CDK4/Cyclin D1 (ProQinase) were used. RB was used as a positive control.

Boiling the samples for 5 min in the presence of denaturing sample buffer stopped the reaction. Samples were subsequently subjected to SDS–PAGE, and transferred to a nitrocellulose membrane before being exposed to an X-ray film at -80°C during 4 hours or over night. Recombinant protein loading was confirmed by SYPRO Ruby protein Blot Staining (Life Technologies).

For mass spectrometry, recombinant kinase dead AMPK trimmers (α2β2γ1) were used as a substrate for CDK4/CyCD3. Recombinant kinase dead AMPK trimers (α2β2γ1) were produced by the DG. Hardie lab.

Mitochondrial isolation

Quadriceps muscle from *Cdk4*$^{+/+}$ or *Cdk4*$^{-/-}$ mice were homogenized in 2ml cold buffer I. Tissue homogenization was obtained at 1500rpm after 30 strokes. The homogenized extract was then centrifuged at 600g for 10 min at 4°C in order to remove cellular debris. This step was performed three times. The mitochondrial fraction was pelleted at 10000g for 10 min at 4°C and subsequently washed using buffer II. The mitochondrial pellet was suspended in 80ul cold buffer II. Mitochondria were immediately used for seahorse analysis. Buffers I composition is as follows: 210 mM mannitol, 70 mM sucrose, 5 mM HEPES, 1 mM EGTA, 0.5% BSA pH to 7.4. Buffer II composition is as follows : 210 mM mannitol, 70 mM sucrose, 10 mM MgCl2, 5 mMK2HPO4, 10 mM MOPS, 1 mM EGTA pH to 7.4.

Isolation of adult skeletal muscle fibers

Flexor digitorum brevis (FDB) muscles were incubated for 45 min at 37°C in an oxygenated 'Krebs-Hepes' solution containing 0.2% collagenase type IV (Gibco). Muscles were then washed twice in DMEM/F12 supplemented with 2% fetal

bovine serum and mechanically dissociated by repeated passages through fire-polished Pasteur pipettes of progressively decreasing diameter. Dissociated fibers were plated directed onto Seahorse XF24 tissue culture dishes coated with Matrigel and allowed to adhere to the bottom of the dish for 2h. After checking the adhesion of the fibers, a seahorse Fatty acid oxidation was performed as described The Krebs-Hepes solution contains NaCl 135.5mM, $MgCl_2$ 1.2mM, KCl 5.9mM, glucose 11.5mM, Hepes 11.5mM and $CaCl_2$ mM.

Seahorse analyses

For seahorse analysis, the cells were seeded 16 hours before the experiment.

Mitochondrial function was determined with an XF-24 extracellular flux analyzer (Seahorse Bioscience). Oxygen consumption Rate (OCR) and Extracellular acidification rate (ECAR) was measured in adherent MEFs. Control and mutant fibroblast cells were seeded in an XF 24-well cell culture microplate at a density of 7×10^5 cells per cell in 200 µL DMEM/F12 media. Cells were incubated for 16 h at 37 °C in 5% CO_2 before the assay. OCR was expressed as pmol of O_2 per minute and was normalized by protein content a Pierce BCA Protein Assay protocol (Thermo Fisher Scientific). ECAR was expressed as mpH per minute and was normalized by protein content a Pierce BCA Protein Assay protocol (Thermo Fisher Scientific).

For glycolysis experiments, just before the experiment the cells were washed, and the growth medium was replaced with DMEM medium containing only 2mM Glutamine**.** Cells were then pre-incubated for 1 h at 37 °C without CO_2 to allow cells to pre-equilibrate with the assay media before starting the glycolysis test procedure. After measuring baseline ECAR, ECAR was measured after an acute injection of 25mM Glucose. The glycolytic rate was calculated as glucose dependent ECAR. It was calculated as follows: Glucose induced ECAR-basal ECAR.

For fatty acid oxidation experiments, just before the experiment the cells are washed, and the growth medium was replaced with KHB containing 2.5mM Glucose and 1.5mM of carnitine**.** Cells were then pre-incubated for 1 h at 37 °C without CO_2 to allow cells to pre-equilibrate with the assay media before starting the fatty acid oxidation procedure. After measuring baseline OCR as an indication of basal respiration, OCR was measured after an acute injection of 400µM or

150µM of palmitate coupled to BSA (for MEFs and myotubes respectively).

For FDB muscle fibers 125µM of palmitate coupled to BSA, 400nM of FCCP and 1µM of Antimycine A were injected directly onto the fibers using the seahorse analyzer. Fatty acid oxidation was induced by the palmitate injection. The uncoupling agent FCCP induced the maximal respiration.

OCR was expressed as pmol of O_2 per minute and was normalized by total DNA content.

For mitochondrial respiration, 50 µl of mitochondrial suspension (containing 10µg of freshly isolated mitochondria) were used per well. The XF24 cell culture microplate was centrifuged at 2000g for 20 minutes at 4 °C. The assay medium contained 250 mM sucrose, 15 mM KCl, 1 mM EGTA, 5 mMMgCl2, 30 mM K2HPO4, 2mM Hepes and 0.2% FFA-Free BSA. 0.5mM Malate, 80µM PalmitoylCoA, 240µM Carnitine and 4mM ADP diluted in assay medium were added after the centrifugation of the mitochondria to obtain a final volume of 525µl per well. After 10 min of incubation at 37°C without CO2 the mitochondrial respiration was measured using the seahorse analyzer.

Immunopreciptation

Myotubes or liquid N2 grinded muscle samples were lysed in M-PER™ buffer (Thermofisher Scientific) and incubated in agitation for one hour at 4°C. 2-5 mg of protein was inmunoprecipitated overnight with an AMPKα2 antibody (Santa Cruz, sc-19131) and Protein G coupled with magnetic beads (Sigma, 1004D) in the following buffer (IP buffer): 25 mM TRIS pH 7.9, 5 mM $MgCl_2$, 10% Glycerol, 100 mM KCl, 0.1% NP40, 0.3 mM DTT. Next day, beads were washed for times with the IP buffer and frozen. Samples were used for mass spectrometry.

Mass spectrometry

In the *in vitro* assays, protein samples were loaded on a 12 % mini polyacrylamide gel and migrated about 3 cm, while in the immunoprecipitation experiments proteins were loaded on an 8% gel and fully migrated. After Coomassie staining, visible band between 50 and 75 kDa corresponding to AAPK2 was excised and digested with sequencing-grade trypsin (Promega). Extracted tryptic peptides

were dried and resuspended in 0.05% trifluoroacetic acid, 2% (v/v) acetonitrile for mass spectrometry analyses.

Tryptic peptide mixtures were injected on an Ultimate RSLC 3000 nanoHPLC system (Dionex, Sunnyvale, CA, USA) interfaced via a nanospray source to a high resolution mass spectrometer based on Orbitrap technology: Fusion Tribrid or QExactive Plus (Thermo Fisher, Bremen, Germany), depending on the experiments considered. Peptides were loaded onto a trapping microcolumn Acclaim PepMap100 C18 (20 mm x 100 µm ID, 5 µm, Dionex) before separation on a C18 reversed-phase analytical nanocolumn at a flowrate of 0.25 µl/min, using a gradient from 4 to 76 % acetonitrile in 0.1 % formic acid (total time: 65min).

The *in vitro* experiments were analysed with a Fusion mass spectrometer interfaced to a custom packed 40-cm C18 column (75 µm ID, 100Å, Reprosil Pur 1.9 um particles). Full MS survey scans were performed at 120'000 resolution. Data-dependent acquisition was controlled by Xcalibur 3.0 software (Thermo Fisher) and applied a top speed precursor selection strategy to maximize acquisition of peptide tandem MS spectra with a maximum cycle time of 3s. Multiple-charge precursor ions were isolated in the quadrupole with a window of 1.6 m/z width and then dynamically excluded from further selection during 60s. HCD fragmentation was performed in the ion routing multipole with 32% normalized collision energy and fragment ions were measured in the ion trap.

The immunoprecipitation experiments were analysed with a Q-Exactive Plus instrument interfaced to an Easy Spray C18 PepMap column (50cm x 75µm ID, 2µm, 100Å, Dionex). Full MS survey scans were performed at 70'000 resolution. In data-dependent acquisition controlled by Xcalibur 3.1 software (Thermo Fisher), the 10 most intense multiple-charge precursor ions detected in the full MS survey scan were selected for higher energy collision-induced dissociation (HCD, normalized collision energy NCE=27 %) and analysis in the orbitrap at 17'500 resolution. The window for precursor isolation was of 1.5 m/z units around the precursor and selected fragments were excluded for 60s from further analysis.

MS data were analysed using Mascot 2.6 (Matrix Science, London, UK) set up to search the UniProt database (www.uniprot.org) restricted to *Homo sapiens* (i*n vitro* experiments) or *Mus musculus* (immunoprecipitation experiments) taxonomy

(SwissProt, November 2016 version: 20'130 and 16'846 sequences, respectively). Trypsin (cleavage at K,R) was used as the enzyme definition, allowing 3 missed cleavages. Mascot was searched with a parent ion tolerance of 10 ppm and a fragment ion mass tolerance of 0.5 (Fusion MS data) or 0.02 Da (QExactive MS data). Iodoacetamide derivative of cysteine was specified in Mascot as a fixed modification. N-terminal acetylation of protein, oxidation of methionine, and phosphorylation of serine, threonine or tyrosine were specified as variable modifications.

Scaffold software (version 4.7.5, Proteome Software Inc., Portland, OR) was used to validate MS/MS based peptide and protein identifications, and to perform dataset alignment. Peptide identifications were accepted if they could be established at greater than 90.0% probability by the Scaffold Local FDR algorithm. Protein identifications were accepted if they could be established at greater than 95.0% probability and contained at least 2 identified peptides. Protein probabilities were assigned by the Protein Prophet algorithm. Proteins that contained similar peptides and could not be differentiated based on MS/MS analysis alone were grouped to satisfy the principles of parsimony. Proteins sharing significant peptide evidence were grouped into clusters.

MsViz software (Martin Campos et al., 2017) was used to compare sequence coverage and phosphorylation of the AMPK alpha 2 protein in the *in vitro* experiments.

HPLC

Cells were grown in 10 cm dishes and treated as indicated in the figure legends. Culture medium was removed by aspiration, rinsed with ultra pure water, flash frozen with liquid nitrogen, thawed on ice, and followed by immediate addition of ice-cold 0.4M perchloric acid (500 µl). Cells were scrapped off thoroughly, and transferred to 1.5-ml microfuge eppendorf tubes. Samples were incubated at 4°C for 45 minutes, and centrifuged at 14,000 rpm at 4C for 10 minutes. The supernatant (500 µl) was collected, mixed with 500µl K_2CO_3 4M, and incubated at least 1h at -80°C. The samples were again centrifugated at 4C for 10 minutes, the supernatant collected and tested on HPLC.

External standards stocks were prepared in ultra pure water, at 10 mg/ml, and

treated in exactly the same way as the samples.

For normalization, protein measurements were performed using a Pierce BCA Protein Assay protocol (Thermo Fisher Scientific). In parallel DNA was extracted from the pellets and quantified.

The gradient elution was performed as described (Manfredi et al., 2002) on a 4.6-mmi.d, 150-mm, Kinetex 5u EVO C18 100A HPLC column (Phenomenex) with two buffers at a rate of 0.5 ml/min. Buffer A contained 25mM NaH2PO4, 100 mg/liter tetrabutylammonium hydrogen sulfate, pH 5. Organic buffer B was composed of 10% (v/v) acetonitrile in 200mM NaH2PO4, 100 mg/liter tetrabutylammonium hydrogen sulfate, pH 4.0. Buffers were filtered and degassed. The gradient was 100% buffer A from 0–5 min, 100% buffer A to 100% buffer B from 5–20 min, and 100% buffer A from 20 to 31 min for column reequilibration, which was sufficient to achieve stable baseline conditions. 25 microliters of prepared sample was autoinjected and UV monitored at 260nm from 0 to 31 min for phosphorylated nucleotides. Peaks were identified by their retention times and by using co-chromatography with standards.

Each standard of interest was first subjected to chromatography individually to obtain its retention time (Manfredi et al., 2002) and to be able to later identify each compound in a standard mixture. A standard curve for each compound was constructed by plotting peakheight s (lV) versus concentration. Linear curves were obtained with R^2 values > 0.95. The quantification of nucleotides in the sample was performed using the external standard calibration, integrating sample peak heights against corresponding standard curves.

mRNA analysis.

Muscle tissues were grinded to powder in liquid nitrogen. mRNAs from muscle was isolated using TRIREAGENT according to the manufacturer's protocol. One microgram of the RNA was subsequently reverse-transcribed (Superscript II, Life Technologies) and quantified via real-time quantitative PCR using an ABI 7900HT instrument. qPCR analysis was performed using a 7900HT Fast Real-Time PCR System (Applied Biosystems) and SYBR Green detection of the amplified products. The relative quantification for a given gene was corrected to RS9 mRNA values (oligonucleotide sequences are provided in Table 3).

QUANTIFICATION AND STATISTICAL ANALYSIS

The results were expressed as means ± standard error of the means (s.e.m). Comparisons between 2 groups were performed with an unpaired 2-tailed Student's *t* test and multiple group comparisons were performed by unpaired 1-way ANOVA followed by Tukey's test and 2-way ANOVA, followed by Tukey's test. All *p*-values below 0.05 were considered significant. Statistical significance values were represented by asterisks corresponding to *p<0.05, **p<0.001, ***p<0.001and ****p<0.0001.

Lopez-Mejia et al, Figure-1

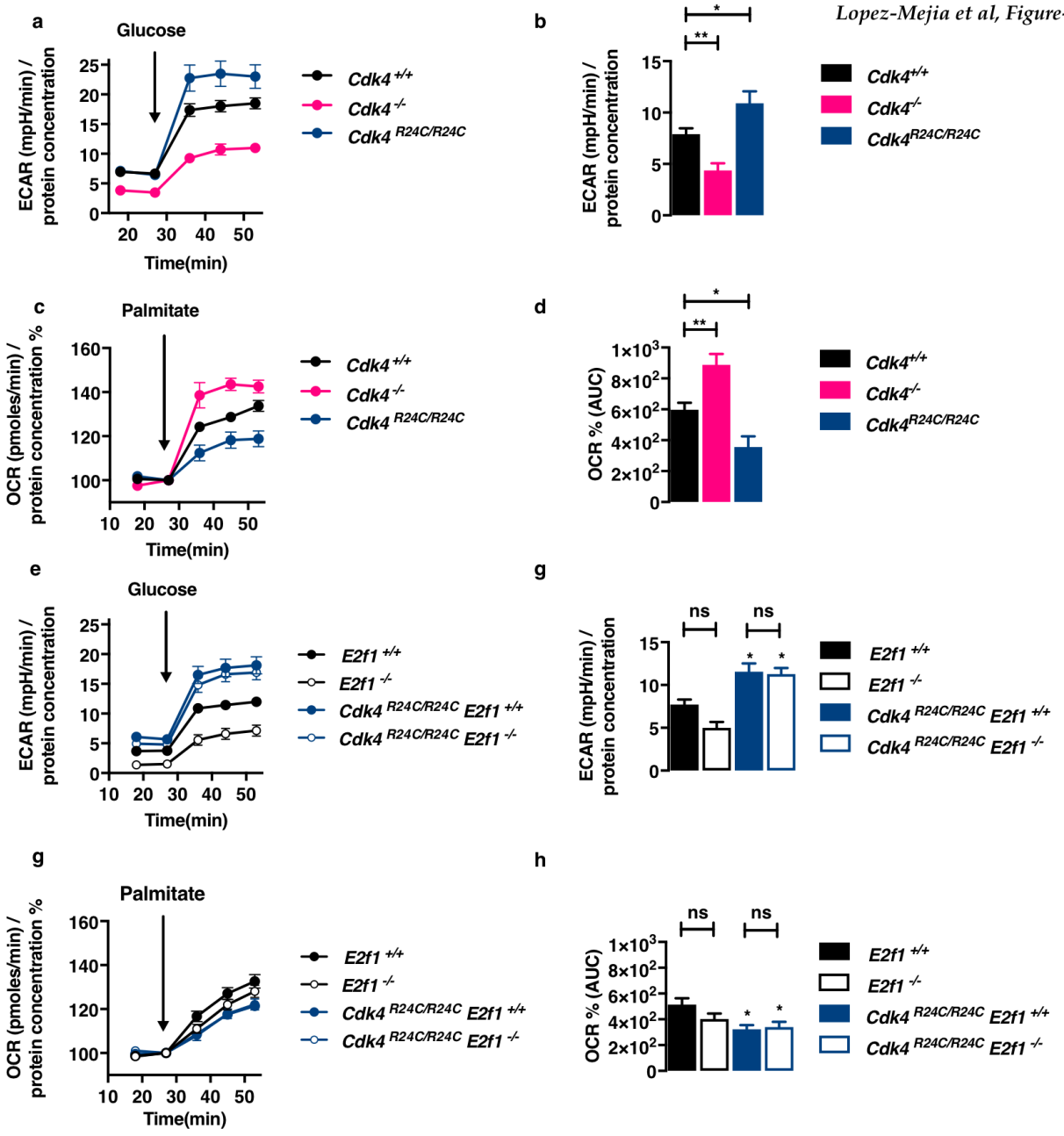

Lopez-Mejia et al, Figure-2

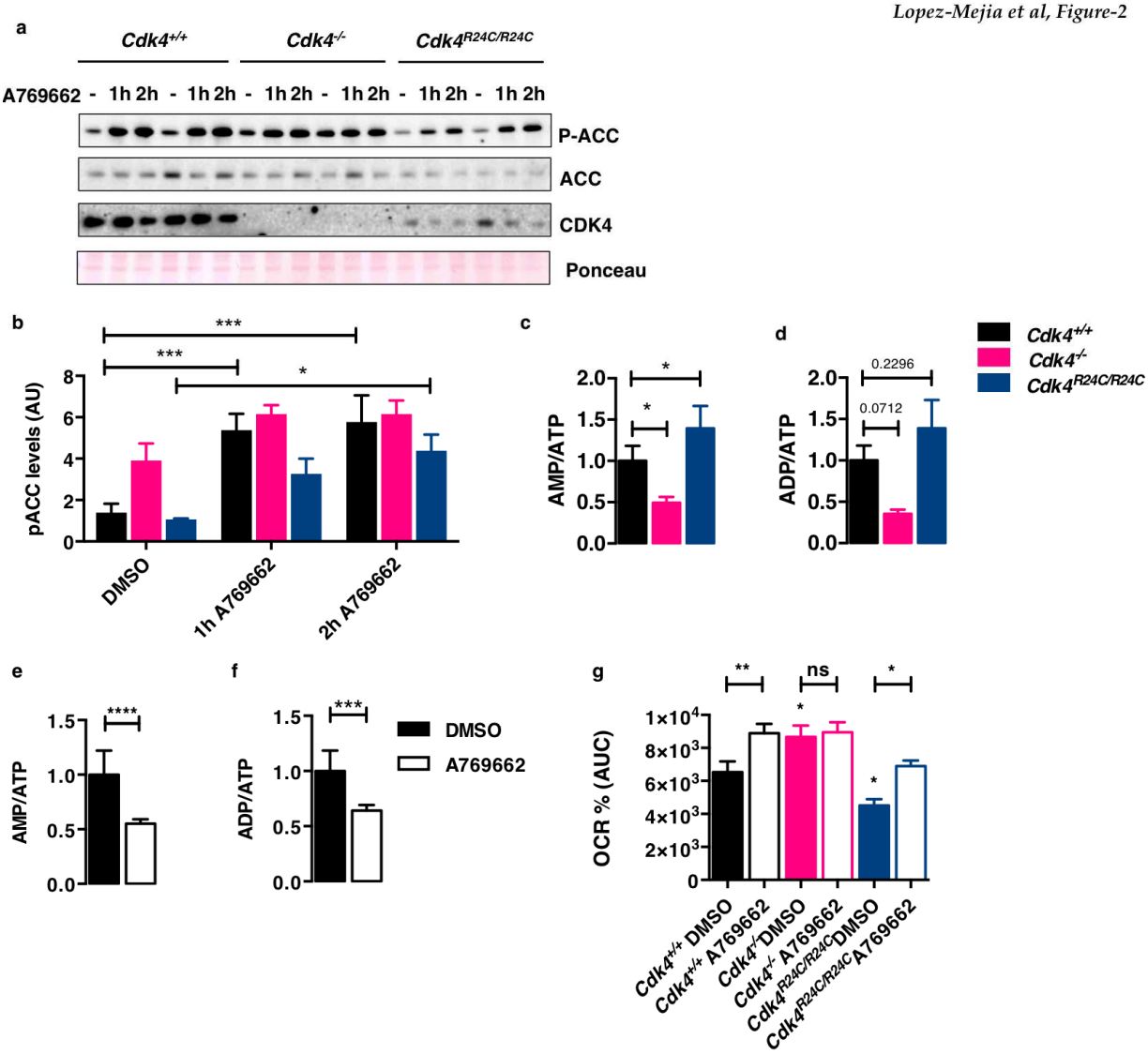

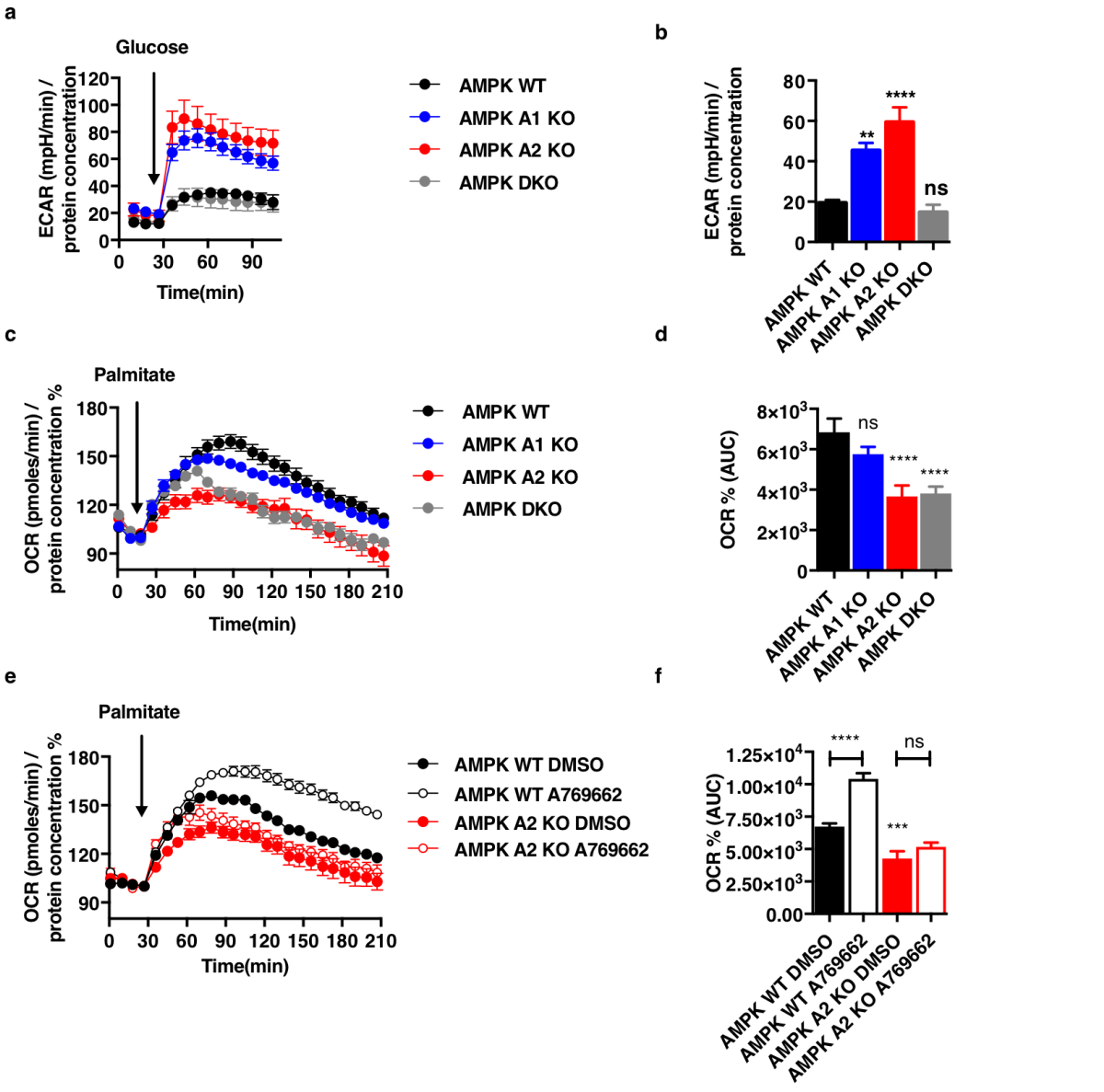

Lopez-Mejia et al, Figure-4

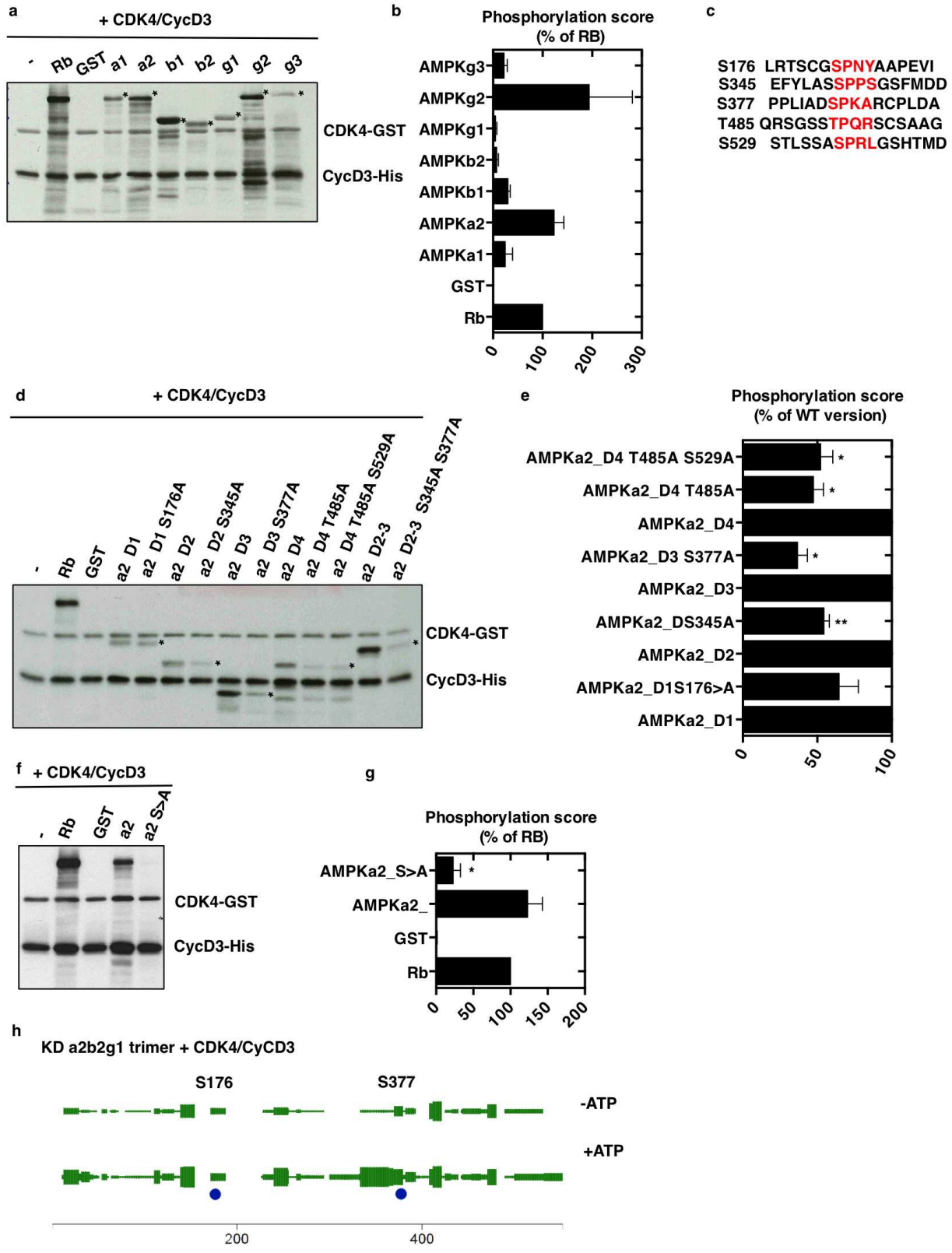

Lopez-Mejia et al, Figure-5

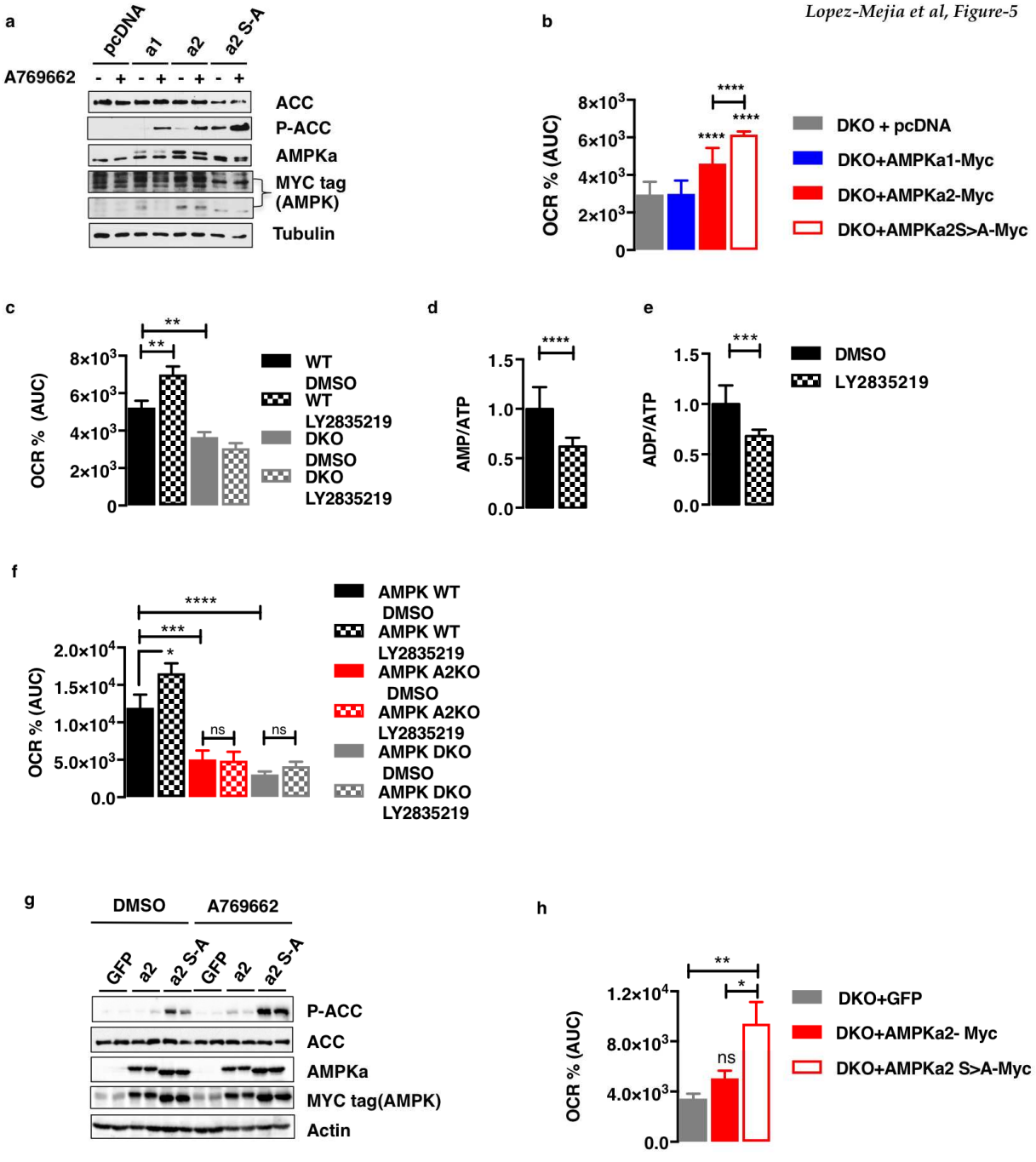

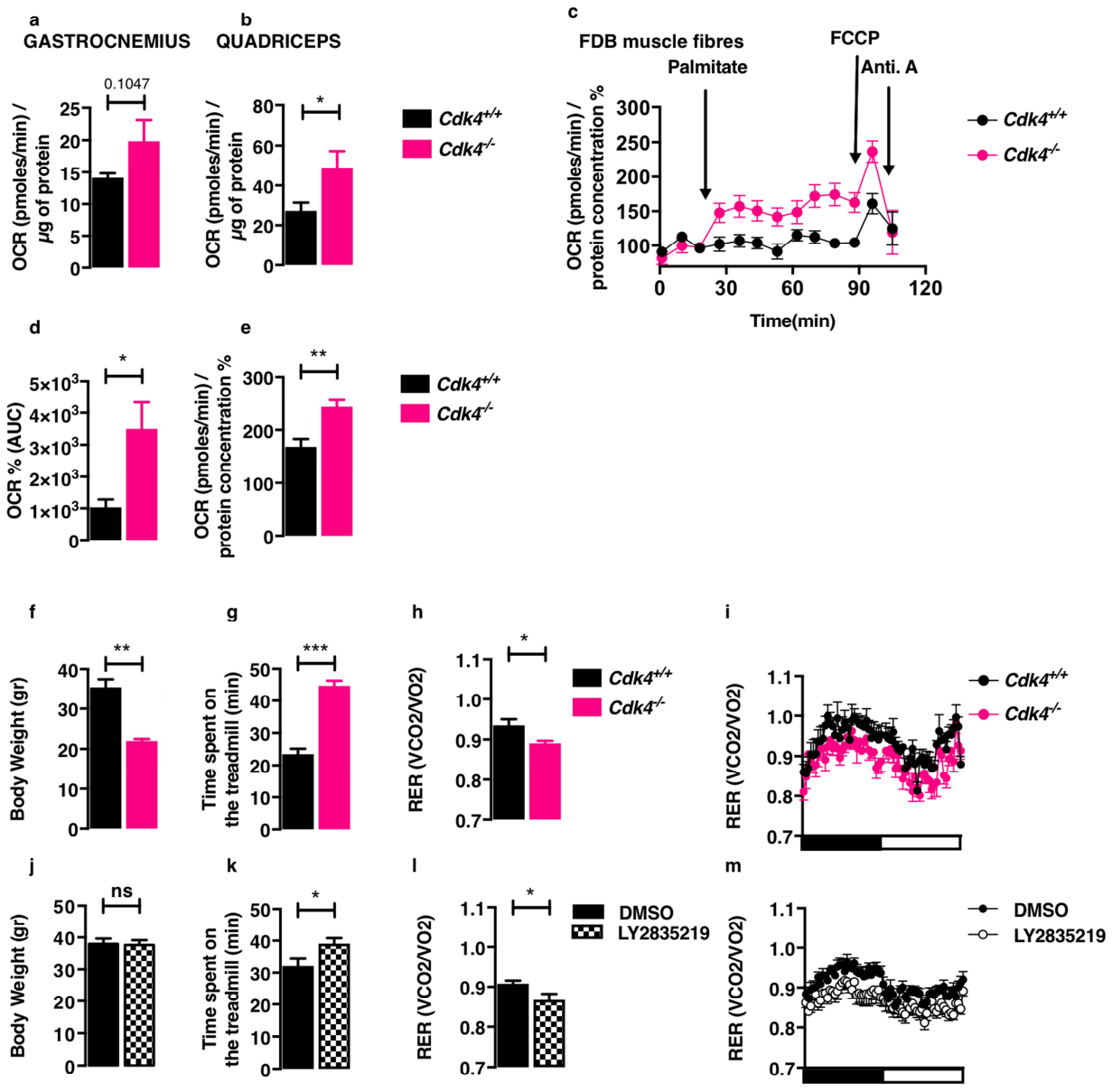

Lopez-Mejia et al, Figure-7